Materials Today Bio 23 (2023) 100889

Contents lists available at ScienceDirect

Materials Today Bio

journal homepage: www.journals.elsevier.com/materials-today-bio

Bifunctional bone substitute materials for bone defect treatment after bone tumor resection

Zhule Wang [a,b], Ingrid CM van der Geest [b,c], Sander CG. Leeuwenburgh [a,b], Jeroen JJP. van den Beucken [a,b,*]

[a] Radboud University Medical Center, Department of Dentistry – Regenerative Biomaterials, Nijmegen, the Netherlands
[b] Research Institute for Medical Innovation, Radboudumc, Nijmegen, the Netherlands
[c] Radboud University Medical Center, Department of Orthopedics, Nijmegen, the Netherlands

ARTICLE INFO

Keywords:
Bone substitutes
Bone tumor
Bone tumor treatment
Residual tumor cells
Local anti-cancer efficacy
Bone regeneration and reconstruction

ABSTRACT

Aggressive benign, malignant and metastatic bone tumors can greatly decrease the quality of patients' lives and even lead to substantial mortality. Several clinical therapeutic strategies have been developed to treat bone tumors, including preoperative chemotherapy, surgical resection of the tumor tissue, and subsequent systemic chemo- or radiotherapy. However, those strategies are associated with inevitable drawbacks, such as severe side effects, substantial local tumor recurrence, and difficult-to-treat bone defects after tumor resection. To overcome these shortcomings and achieve satisfactory clinical outcomes, advanced bifunctional biomaterials which simultaneously promote bone regeneration and combat bone tumor growth are increasingly advocated. These bifunctional bone substitute materials fill bone defects following bone tumor resection and subsequently exert local anticancer effects. Here we describe various types of the most prevalent bone tumors and provide an overview of common treatment options. Subsequently, we review current progress regarding the development of bifunctional bone substitute materials combining osteogenic and anticancer efficacy. To this end, we categorize these biomaterials based on their anticancer mechanism deriving from i) intrinsic biomaterial properties, ii) local drug release of anticancer agents, and iii) oxidative stress-inducing and iv) hyperthermia-inducing biomaterials. Consequently, this review offers researchers, surgeons and oncologists an up-to-date overview of our current knowledge on bone tumors, their treatment options, and design of advanced bifunctional biomaterials with strong potential for clinical application in oncological orthopedics.

1. Introduction

Cancer is a leading cause of human death, responsible for 1 out 6 deaths globally in 2018 [1]. With the modernization of society and the improvement of living standards, many risk factors and external stimuli, including obesity, irregular diet, social psychological stress, smoking, drug abuse and air pollution, have increased the prevalence of cancer [2]. In 2019, more than 16.9 million people in the US alone were diagnosed with cancer, and this number is estimated to reach 22.1 million per annum by 2030 [3]. The most prevalent cancers include lung, prostate, breast, colorectal and liver cancers. Although bone cancers occur less frequently, malignant bone tumors are quite lethal and malignant primary bone tumors occur disproportionally often in young people [4].

Despite the low prevalence of primary bone cancers (corresponding to ~1% of all cancers [5]), bones are the most common metastatic site for primary cancers originating elsewhere in the human body [6]. The incidence of bone metastases varies with the type of primary malignant cancer, for which the incidence of bone metastases was 88.7% for patients with primary prostate cancer and 53.7% for patients with primary breast cancer, respectively [7]. Additionally, the incidence of bone metastases among patients with primary malignant lung cancer ranged from 4.1% to 36.9% for different lung cancer subtypes [8].

Primary bone tumors and bone metastases can increase the risk of serious skeletal-related complications, such as pain, joint movement disorders and pathological fractures, and hence seriously impair a patient's quality of life [9–11]. Primary bone tumors and bone metastases can further decrease the mechanical and functional quality of the bone

* Corresponding author. Dentistry - Regenerative Biomaterials (309), Radboud University Medical Center, Philips van Leydenlaan 25, 6525, EX, Nijmegen, the Netherlands.
E-mail address: jeroen.vandenbeucken@radboudumc.nl (J.JP. van den Beucken).

https://doi.org/10.1016/j.mtbio.2023.100889
Received 7 June 2023; Received in revised form 27 October 2023; Accepted 27 November 2023
Available online 1 December 2023

[12,13]. Consequently, patients suffering from malignant bone tumors and bone metastases are more susceptible to pathological bone fractures, severe anemia, loss of appetite, fever, and weight loss, all of which seriously affect the quality of life and survival rate for the patient.

2. Primary and secondary bone cancers

Bone cancers can be generally divided into two categories: primary bone tumors and secondary bone tumors [14]. Primary bone tumors originate from bone tissue itself or its surrounding tissues. In contrast, secondary bone tumors develop from metastasizing cancers originally established in other tissues elsewhere in the body [15] (Fig. 1). Primary bone tumors can be further classified into three types: benign bone tumors, aggressive benign bone tumors and malignant bone tumors. Common benign bone tumors are neither locally invasive nor metastatic. In most cases, patients suffering from common benign bone tumors are asymptomatic and only show clinical symptoms when mechanical-overloading complications occur [16]. The most common types of benign bone tumors are osteoid-osteoma and osteochondroma. Differently, aggressive benign bone tumors can lead to lytic bone lesions, bone expansion, and rarely invade the local surrounding tissues. The invasive capacity of aggressive benign bone tumors is intermediate between non-invasive common benign bone tumors and invasive malignant bone tumors. One of the most prominent representatives of aggressive benign bone tumors is the giant cell tumor of bone (GCT) [17]. Malignant bone tumors display characteristics of distant metastases. Moreover, malignant bone tumors are highly fatal. Before the advent of adjuvant chemotherapy, the overall 5-year survival rate for patients suffering from malignant bone tumors was less than 20% [18]. However, with the development of advanced adjuvant chemotherapy, surgery and imaging techniques, the overall 5-year survival rate for these patients has meanwhile increased to 53–65% [19,20].

The three common types of primary bone tumors have different preferential sites. Benign bone tumors such as osteoid-osteoma and osteochondroma usually establish in the lower limbs [21]: half of the osteoid-osteomas establish in the femur and tibia [22], and osteochondroma predominantly establishes in the metaphysis of the long tubular bones such as the distal femur and proximal tibia. For aggressive benign bone tumors like GCT, the most common sites are the distal femur, proximal tibia, and distal radius. Aggressive benign bone tumors can cause bone lesions in the metaphysis of long bone and invade the subchondral bone [23]. Additionally, malignant bone tumors mostly occur in the femur and tibia, which can cause massive bone lesions and progressively invade the surrounding soft tissue. Imaging-based examination is the dominant diagnostic method for primary bone tumors [24]. Most of the benign bone tumors can be diagnosed by characteristic appearance via x-ray imaging without the need for a biopsy for verification [25]. Computed tomography (CT) and magnetic resonance imaging (MRI) are more frequently used in the diagnosis of malignant bone tumors [26,27]. MRI is mainly used to determine the local extent and surgical stage of a malignant bone tumor [28], which is critical to the operative design for tumor resection [29,30]. High resolution CT-imaging can aid surgeons in grading malignant bone tumors and detecting initial metastatic lesions [31,32]. Furthermore, after surgical tumor resection, the use of MRI and CT allows for monitoring the local tissue response to postoperative chemotherapy and the detection of local tumor recurrence [33,34].

Secondary bone tumors arise from metastasizing cancers derived from other tissues elsewhere in the body. Secondary bone tumors are by far the most common type of malignant tumors treated by orthopedic surgeons [35]. In contrast to the ~10.000 new cases of primary bone tumors each year, over 1.000.000 new patients are diagnosed with

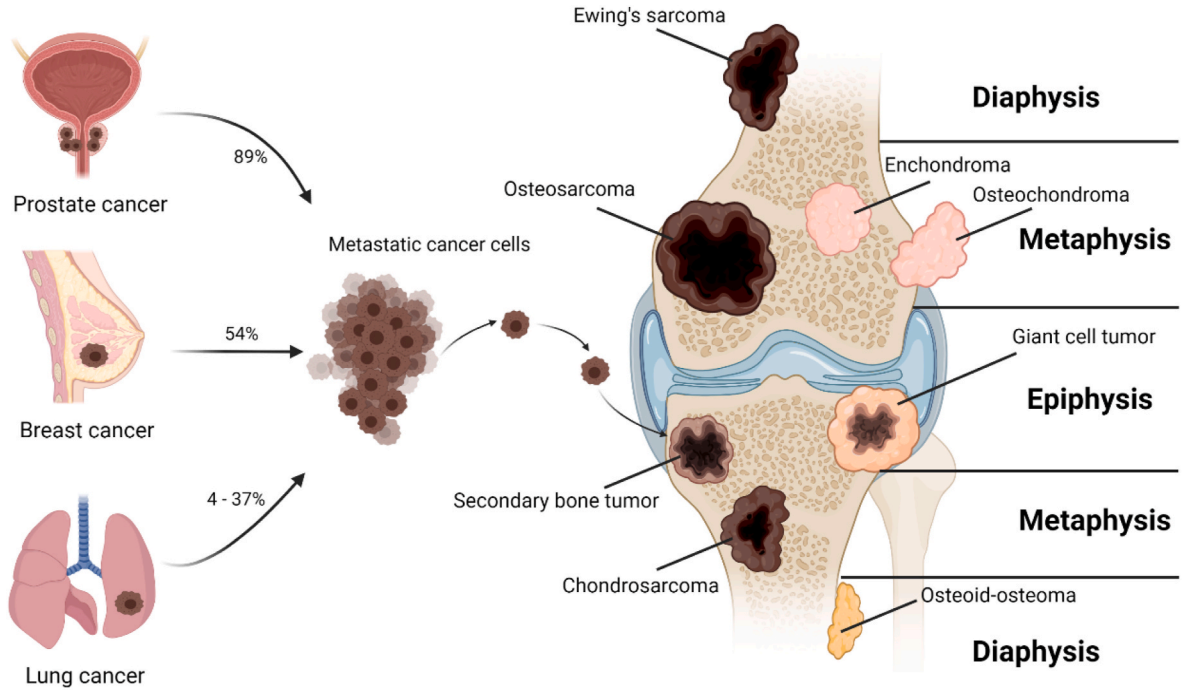

Fig. 1. Schematic representation of common primary bone tumors, secondary bone tumors, and their typical prevalence at different locations in long bones. Common primary bone tumors can be categorized into benign bone tumors (osteoid-osteoma, enchondroma and osteochondroma), aggressive benign bone tumor (giant cell tumor) and malignant bone tumors (osteosarcoma, Ewing's sarcoma, and chondrosarcoma). Osteoid-osteoma is an osteogenic bone tumor that is composed of bone-like tissue and immature trabecular bone, and occurs in the diaphysis of the femur and tibia. Enchondroma and osteochondroma are mainly composed of immature cartilaginous tissue and malformed cortical bone, and mainly occur in the metaphysis of long tubular bone (distal femur or proximal tibia). Giant cell tumor is an osteolytic bone tumor which can cause local malignant transformation or lung metastasis, and occurs in the epiphysis of the femur and tibia. Primary malignant bone tumors such as osteosarcoma, chondrosarcoma and Ewing's sarcoma are not only osteolytic and locally invasive, but also distantly metastatic, which mostly occur in the femur and tibia. Common secondary bone tumors arise from metastasizing prostate, breast and lung cancers (89%, 54% and 4–37%, respectively), and generally occur in distal femur and proximal tibia (created in BioRender.com).

common cancers every year in US, and more than 50% of these latter patients will develop bone metastases before they die [6,36,37]. Most secondary bone tumors originate from metastasizing prostate or breast cancers, and to a lesser extent from lung and kidney cancers [8]. Current options for treatment of bone metastases are only temporarily effective, because metastatic disease is ultimately an incurable condition and current treatments are only palliative.

3. Current standard-of-care for bone tumor treatment

After confirmation of the diagnosis of a primary bone tumor based on typical symptoms and radiological investigations, surgical staging of bone tumors is often evaluated by a multidisciplinary team consisting of a surgeon, radiologist, pathologist and oncologist to define the optimal treatment strategy [38] (Fig. 2). Tumor curettage is usually performed to treat benign bone tumors, either or not in combination with bone grafting (with e.g. autogenous or allogeneic bone) or bone substitution (i.e. with a biomaterial) to stimulate regeneration of bone in the defect created by tumor curettage [39,40]. The use of autogenous or allogeneic bone can result in excellent bone repair, but complete bone healing and restoration of skeletal functionality may take between 6 and 12 months [41]. With the emergence of (synthetic) bone substitute biomaterials, polymeric bone cement has become the most commonly used biomaterial in orthopedics to fill bone defects resulting from tumor curettage [42]. Polymeric bone cement has several advantageous properties, including the heat resulting from the exothermic polymerization and the toxicity of unreacted monomer that can kill residual tumor cells. Evidently, these properties may also affect healthy cells in an undesired manner. Mechanically, polymeric bone cement is strong and can interlock with the bone cavity wall to enable functional mechanical loading of the affected bone almost immediately after surgery [43,44]. Owing to these favorable features, polymeric bone cements can reduce local recurrence rate and concomitantly enable patients to instantly resume their normal life. The early mechanical loading can shorten the recovery period and achieve appropriate functional outcome [45,46].

For treatment of primary malignant bone tumors, the available surgical methods can be divided into amputation (complete removal of a body part affected by unremovable tumors) and limb salvage treatment (partial removal of the bone involved with the tumor and some of the surrounding tissues). Before the 1970s, tumor recurrence rate after limb salvage treatment was very high, and the 5-year survival rate was less than 20%. Therefore, malignant bone tumors were mainly treated by amputation. Since then, chemotherapeutic treatment (ChT) has fortunately progressed thanks to drugs such as adriamycin (ADR) and methotrexate (MTX), which were preoperatively or postoperatively used following surgical resection of malignant bone tumors [47]. In the 1980s, adjuvant ChT was developed to further prevent tumors from reoccurring [48]. Moreover, more clinical practice-based studies have proven that limb salvage therapy is effective resulting in decrease of local recurrence rates to 5%–10%, which is almost similar to amputation treatment. Therefore, limb salvage surgery combined with systemic ChT or radiotherapy (RT) has gradually become the mainstay in the treatment of primary malignant bone tumors.

Treatment of patients with metastatic bone tumors is more complicated and has a different purpose compared to treatment of primary bone tumors. For patients suffering from metastatic bone tumors, palliative treatment mainly aims to reduce pain and maintain patient mobility and functioning to enable patients to live independently and

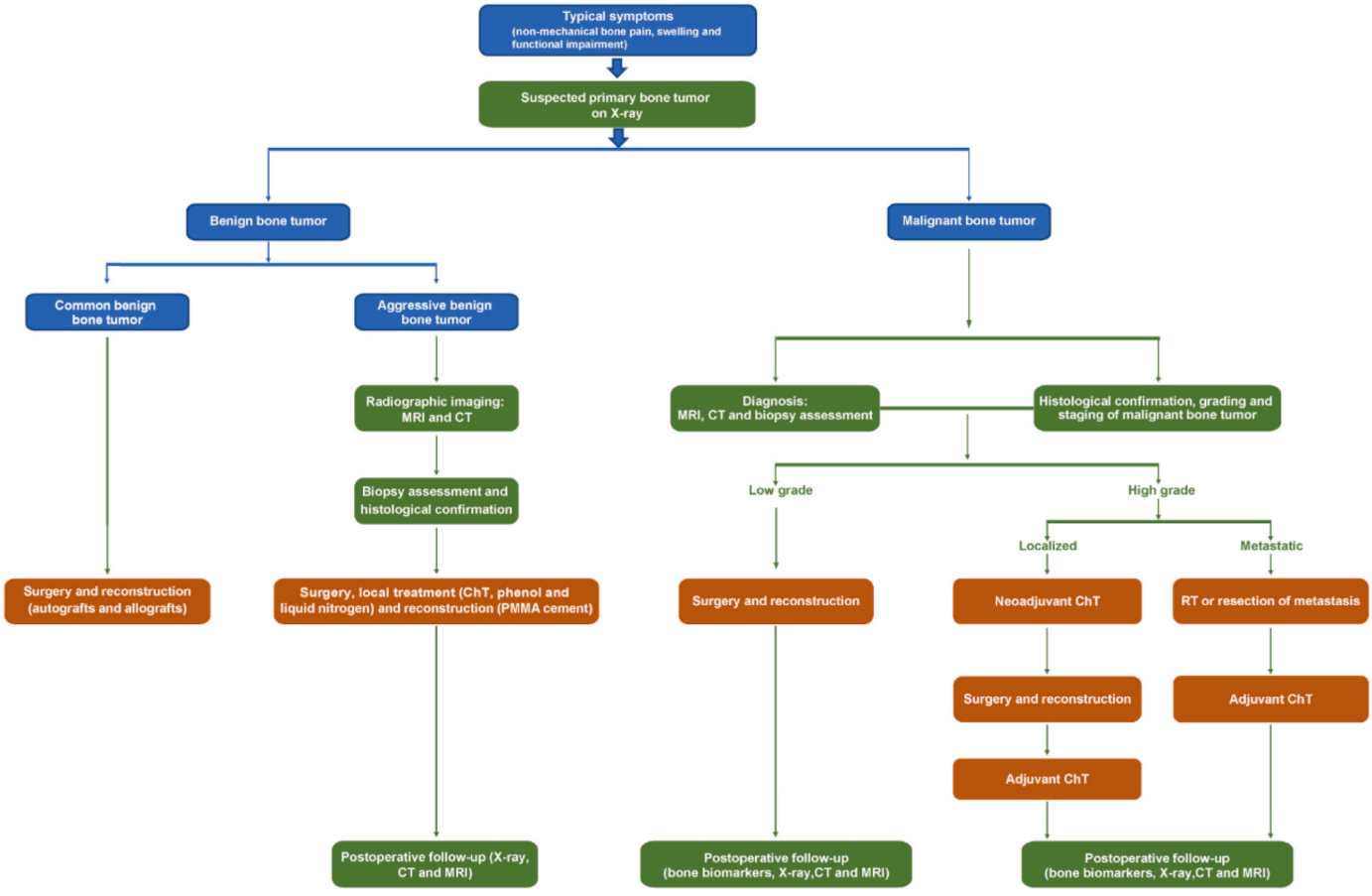

Fig. 2. Flow-chart of the general diagnostic and therapeutic strategy for clinical treatment of primary bone tumors. The typical symptoms and classifications of bone tumors are displayed in blue boxes; Imaging and pathological pre- and post-operative diagnostic methods are displayed in green boxes; Surgical, chemotherapeutic and radiation treatment of bone tumors are displayed in orange boxes.

improve their overall quality of life [49,50]. In some cases, bone metastases require comprehensive treatment, in which first systemic chemotherapy is used, and then a surgical intervention is performed [51]. After surgical intervention, postoperative ChT or RT will be selectively performed based on the specific type of primary tumor and the general physical condition of the patient. Since it is impossible to predict survival times of patients suffering from bone metastases, the surgical design is particularly vital. For metastatic lesions with clear margins after preoperative adjuvant ChT, surgical resection and reconstruction of the resultant bone defect are feasible. For metastatic lesions unsuitable for surgery, RT alone is recommended for pain relief, although this treatment does neither restore bone stability nor prevent pathological bone fractures. Additionally, for patients with a short-term life expectancy, patients should not be left in bed meaninglessly for prolonged periods of time. For these patients, a prosthesis or an intramedullary nail is preferred to achieve bone stabilization, which enables the patient to regain immediate full weight-bearing mobility [52,53], which gives a huge increase of their quality of life.

4. Designing biomaterials with combined bone-regenerative and anti-cancer efficacy

Bone grafts are widely used especially in oncological, traumatic, and prosthetic implantation surgery. Surgical resection of bone tumor tissue often results in bone defects that require reconstructive surgery using bone grafts. Currently, cancellous bone autografts are still the gold standard in regenerative bone surgery. However, the amount of available bone autograft is typically rather limited, and the additional surgery required for bone harvesting often leads to donor site morbidity. Consequently, autologous bone is mainly used for regeneration of relatively small bone defects after curettage or resection of small benign bone tumors. For regeneration of large bone defects resulting from malignant bone tumor resection, several commercially available allografts (e.g. Bone Bank™ Allograft and Stryker® Bio Implant) [54,55] and xenografts (e.g. Pro Osteon® and Bio-Oss®) have been clinically used [56,57]. Although the source of these bone grafts varies, their clinical application is still restricted due to their inherent disadvantages including high cost, risk of disease transmission, low mechanical strength (as freeze-dried or demineralized material), and limited osteogenic capacity.

In addition to these natural bone grafts, various synthetic biomaterials have been developed as bone substitutes with virtually unlimited availability. However, research on their application as bone substitutes to fill defects created by surgical bone tumor resection is still in its infancy [58]. Generally, these biomaterials are either ceramic-based or polymer-based. Ceramic-based biomaterials (e.g. blocks, granules, and cements), most notably calcium phosphate (CaP) ceramics, are chemically very similar to bone mineral, biocompatible, reliable and safe for clinical bone regenerative applications [59–61]. Several types of porous ceramic granules have been used to fill bone defects after resection of benign tumors, leading to satisfactory clinical outcomes [62–64]. Despite their favorable biological properties, poor mechanical properties impede clinical application of these bioceramics in heavily loaded skeletal sites. Similarly, many biodegradable polymer-based materials such as collagen and poly(lactic-co-glycolic acid) (PLGA) are promising candidate materials for treatment of bone defects, but their mechanical performance is also insufficient for application in load-bearing sites [65,66].

After resection of a malignant bone tumor, tumor recurrence is a major risk factor, with local recurrence rates of at least 10% [67,68], which is caused by the fact that not all tumor margins can be cleanly resected by surgery. Subsequent systemic administration of ChT drugs does not reach therapeutically effective concentrations in targeted bones after surgery due to poor blood supply [69,70], implying that residual tumor cells are not completely eliminated. Consequently, ideal biomaterials for filling bone defects resulting from surgical bone tumor resection should be able to support bone reconstruction/regeneration and simultaneously reduce the risk of bone tumor recurrence [71]. The past decades have witnessed the development of novel biomaterials which might act as such bifunctional bone substitutes with the ability to simultaneously support bone formation and locally eliminate residual cancer cells. Therefore, we conducted a review of the available literature on the development of such bifunctional bone substitutes based on specific search strategies with clearly defined inclusion and exclusion criteria. Based on this literature search, we concluded that four main strategies have been followed to date: i) exploiting intrinsic anticancer properties, ii) adding anticancer agents, iii) incorporating agents that induce oxidative stress, or iv) incorporating agents that induce hyperthermia (Fig. 3).

4.1. Search strategy

The literature on bifunctional biomaterials combining bone regenerative capacity and anticancer efficacy was collected by completing a comprehensive and exhaustive search using the following 2 databases: PubMed and Web of Science. The Web of Science was searched for eligible articles using the following keywords: bone tumor treatment, biomaterial and regeneration, while PubMed was searched for eligible articles using the following MeSH terms: ((((Bone Neoplasm*[tiab] OR Bone Cancer*[tiab] OR Cancer* of the Bone[tiab] OR Cancer* of Bone [tiab]) OR ("Bone Neoplasms"[Mesh:NoExp])) AND ((Therapeutic[tiab] OR Therapy[tiab] OR Therapies[tiab] OR Treatment*[tiab]) OR ("Therapeutics"[Mesh:NoExp]))) AND ((Bone Regeneration*[tiab] OR Osteoconduction[tiab]) OR ("Bone Regeneration"[Mesh:NoExp]))) AND ("Animals"[Mesh:NoExp]). All references listed in the results were hand-searched to exclude studies not meeting the eligibility criteria of the current study.

4.2. Inclusion and exclusion criteria

The study selection was limited to research articles that: i) include both *in vivo* and *in vitro* anticancer studies and ii) *in vitro* or *in vivo* osteogenesis evaluation of the biomaterials. The research articles reporting only anticancer or osteogenesis assessment of biomaterials were excluded.

4.3. Bone-substituting biomaterials with intrinsic anticancer efficacy

Commonly used polymeric or bioceramic biomaterials such as chitosan (CH) and nano-sized hydroxyapatite (HA) were recently claimed to exhibit intrinsic anticancer efficacy. CH is a polymer composed of glucosamine and N-acetylglucosamine [72] and derived from chitin. This natural polymer is widely used in bone regenerative research due to its biocompatibility, biodegradability and hydrophilicity [73–75]. Interestingly, CH was shown to induce apoptosis in human osteosarcoma cells (Saos-2) via caspase-2 and -3 activation *in vitro*, while it inhibited angiogenesis for tumor growth [76]. Additionally, CH plays a synergistic anti-cancer role via immune cells, as demonstrated by its induction of monocyte differentiation into dendritic cells (DCs) and their enhanced secretion of interleukin-12 (IL-12). IL-12 activates T cells to secrete cytokines that stimulate host anticancer immunity to reduce the incidence of bone metastasis from lung cancer in mice [77].

HA has the chemical formula $Ca_5(PO_4)_3(OH)$ corresponding to a stoichiometric Ca/P ratio of 1.67. This bioceramic is routinely applied in clinics as filling material for regenerative orthopedic applications [78]. A recent study reported that nano-sized HA (n-HA) exhibits intrinsic anticancer activity [79]. Rod-shaped n-HA was easily internalized into metastatic squamous carcinoma cells, activating their mitochondrial apoptotic pathway *in vitro*. In combination with titanium scaffolds this nano-sized HA effectively treated tumor-associated segmental bone defects in rabbits. Most importantly, n-HA showed a pro-apoptotic effect on malignant tumor cells but did not negatively affect fibroblasts.

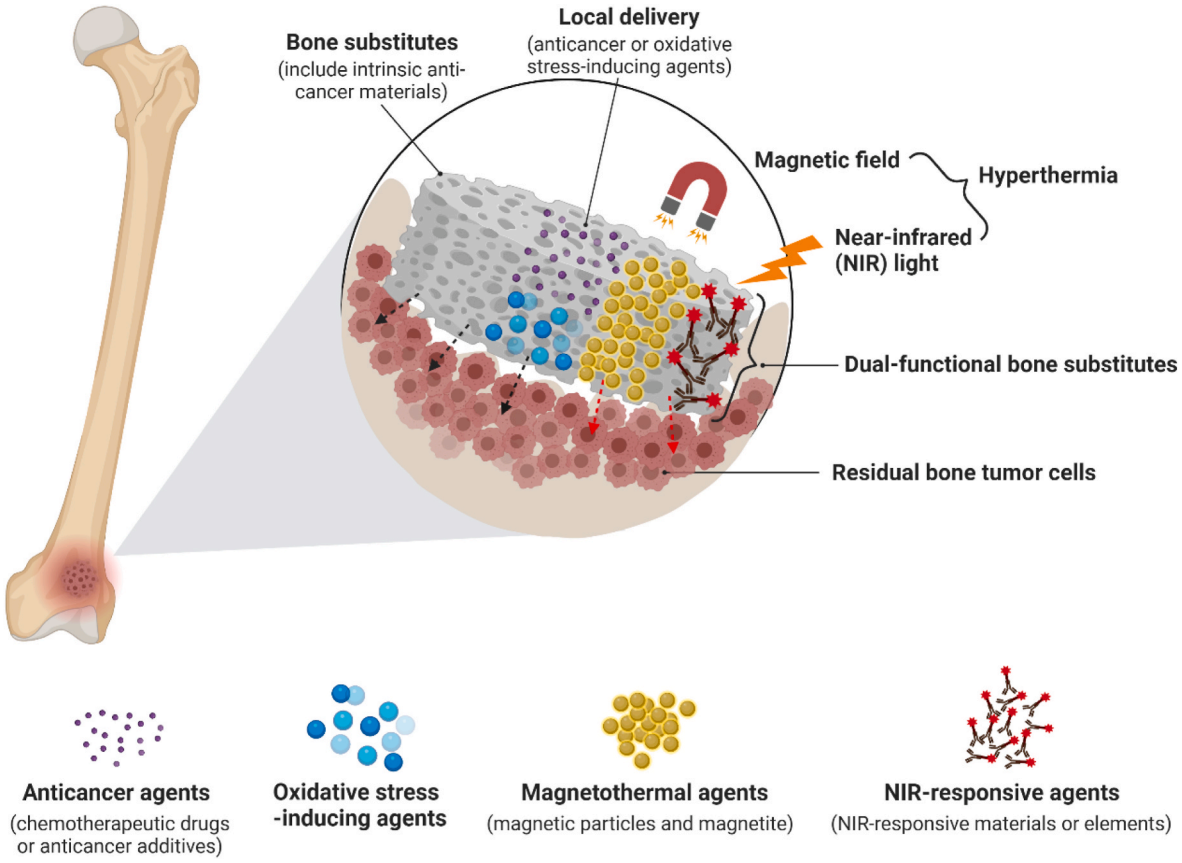

Fig. 3. Current design strategies to develop bifunctional bone substitutes simultaneously promoting bone regeneration and killing cancer cells. Development of bifunctional bone substitutes by i) using intrinsic anticancer materials, ii) adding anticancer agents (including chemotherapeutic drugs and anticancer additives), iii) agents inducing oxidative stress, or iv) agents inducing hyperthermia (including magnetic particles and NIR-responsive materials and elements) to bone substitutes (created in BioRender.com).

4.4. Addition of anticancer agents

The most commonly explored strategy to render bone substitutes active against cancer cells involves their combination with either established anticancer agents (e.g. ChT drugs) which are already used in clinics or novel experimental anticancer agents. The release of these anticancer agents occurs via desorption, concomitant with (partial) bone substitute degradation, or on demand, upon which the anticancer agents can exert its detrimental effect on bone tumor cells around the bone defect after bone tumor resection.

ChT drugs are generally categorized according to their anticancer mechanism, including cytotoxic drugs, hormonal drugs, biological response modifiers, monoclonal antibody drugs, and other adjuvant drugs (Table 1). Cytotoxic drugs play a predominant role in the treatment of bone malignancies, and hence have been frequently used in combination with bone substitutes to allow for treatment of bone tumors via local drug delivery [80,81] (Table 2). These drugs can exert anti-cancer effects by entering the tumor cell nucleus and affecting the structure of cellular DNA, thereby interfering with nucleic acid synthesis and transcription. Physical approaches such as adsorption and freeze-drying are the most common methods to load chemotherapeutic drugs onto bone-substituting biomaterials due to their simplicity and

Table 1
Common chemotherapeutic drugs used for systemic treatment of bone tumors.

Categories	Representative drugs	Mechanisms of action	Indications	Major side effects
Cytotoxic drugs	Cyclophosphamide, doxorubicin, methotrexate, adriamycin, cisplatin, paclitaxel	Affect the chemical structure of cellular DNA, interfere with nucleic acid synthesis and transcription	Malignant and metastatic bone tumors	Abnormal hematopoiesis, cardiomyopathy, weight loss, renal dysfunction, ototoxicity
Hormone drugs	Tamoxifen, megestrol, goserelin	Interfere with binding of hormones and their receptors, inhibit the growth of hormone-related tumors	Metastatic bone tumors caused by breast cancer or prostate cancer	Fever, depression, hypertension, abnormal liver function
Biological response modifiers	Interferon, interleukin-2, thymosin	Increase the differentiation and activity of T cells, B cells and macrophages in the autoimmune system	Osteosarcoma, metastatic bone tumors caused by breast cancer	Fever, endocrine dysfunction, abnormal blood biochemical indicators
Monoclonal antibody drugs	Bevacizumab	Inhibit the biological effects of VEGF, thereby inhibiting tumor angiogenesis, growth and metastases	Metastatic bone tumors caused by lung cancer	Gastrointestinal perforation, hemorrhage, arteriovenous thrombosis
Adjuvant drugs	Erythropoietin, morphine, pamidronate disodium	Inhibit the activity of osteoclasts, analgesic effects or pain caused by osteolytic bone metastases	Hypercalcemia, pain, bone destruction and dissolution caused by malignant tumor and bone metastases	Hypocalcemia, fever, inhibition of the central nervous system

Table 2
Bifunctional biomaterials fabricated by incorporation of anticancer agents.

Building block materials	Anti-cancer agent	Fabrication method	Local delivery form	Drug release time	*In vitro* therapeutic efficiency	Osteogenesis or biocompatibility assessments	*In vivo* bone tumor model	Initial tumor volume and *in vivo* therapeutic efficacy	Ref.
Polycaprolactone (PCL)	Doxorubicin	Freeze drying	3D-printed scaffold	Up to 84d	Dose-dependent cytotoxic effects; around 60% viability for high loading and 75% for low loading groups on breast cancer cells after 3d	No detected cardiotoxicity	3×10^6 231-luc cells - subcutaneous tumor model in mice	200 mm^3; Tumor volume decreased from over 1500 mm^3 to smaller than 500 mm^3	[83]
HA	Doxorubicin	Adsorption	Nano or micro-sized HA	72h	Dose-dependent increase in cellular uptake of nHA + DOX and cytotoxic effects on 143B cells	Nano/micro-HA particles were less cytotoxic to MC3T3 cells compared to nHA alone	2×10^6 143B cells - subcutaneous tumor model in mice	Tumor volume increased to only 500 mm^3 in nano/micro-HA + DOX group compared to 2500 mm^3 in the control	[84]
β-TCP and black phosphorous nanosheets	Doxorubicin	Freeze dying	Porous scaffold	14d	Complete elimination of MG-63 cells in DOX/P24/BP/TCP/PLGA (BDPTP) and BP/P24/TCP/PLGA (BPTP) scaffolds groups after 1d	BDPTP and BPTP scaffolds supported the proliferation of rBMSCs and increased ALP activity *in vitro*; Promoted new bone formation of the cranial defects in rats	1×10^7 MG-63 cells - subcutaneous tumor model in mice	200 mm^3; Tumor volume decreased from 200 to 0 mm^3 at day 4 for BDPTP and BPTP groups	[85]
PLLA	CD40 antibody	PDA motif-mediated crosslinking reaction	Fibrous scaffold	3d	Efficiently induced MDA-MB-231 cell apoptosis	No cytostatic effects on MC3T3-E1 cells *in vitro*	2×10^6 MDA-MB-231 cells - ectopic humanized breast tumor in axillary region of mice	27 mm^3; Tumor volume was significantly suppressed to around 50 mm^3 in PLLA-PDA-CD40mAb group compared to around 800 mm^3 in the control group	[86]

easy handling.

Doxorubicin (DOX) is a commonly used anthracycline anticancer drug in clinics [82], and has also been frequently combined with various biomaterials to combat bone tumors [83–85]. DOX was loaded on polycaprolactone (PCL), micro/nano-sized HA or 2D black phosphorus (BP) scaffolds via adsorption, resulting in sustained release of 58.7% (PCL), 80% (HA) or 26% (BP) after 84 days, 72 h and 14 days, respectively. Moreover, the released DOX showed dose-dependent cytostatic effects on human metastatic breast cancer cells and osteosarcoma cells *in vitro*. In addition, when DOX was loaded onto nHA, the DOX-loaded nHA was internalized by cells and delivered to lysosomes, after which DOX accumulated in mitochondria and caused dysfunction of mitochondria to inhibit tumor cell proliferation.

DOX-loaded biomaterials were further implanted and tested in subcutaneous bone tumor models. Xenograft tumor models are generally developed by subcutaneously injecting tumor cells (e.g. osteosarcoma cells and metastatic bone tumor cells) into the flank or back of mice. After the tumor volume reaches a certain level (80–200 mm^3), the tumor models were used for *in vivo* evaluation of tumor therapy. Sun et al. found that the DOX-loaded PCL scaffolds resulted in a significant inhibition of tumor growth *in vivo* (only a 250% increase in volume), while the tumor volume increased 650% in the controls within 28 days. Additionally, Wang et al. demonstrated that DOX-loaded scaffold achieved a long-term prevention of tumor recurrence in subcutaneous tumor-bearing mice models.

Due to the high cytotoxicity of DOX to healthy cells, systemic administration of DOX can induce severe adverse side effects including nephrotoxicity, cardiotoxicity and immune suppression. Regarding bone regenerative application after bone tumor resection, elimination of tumor cells by DOX should not lead to severe detrimental effects on healthy bone cells. Notably, the sustained release of the anticancer agents after combining with the biomaterial significantly reduced the local toxicity for bone repair and systemic toxicity for metabolic organs. As shown by Sun et al., the local delivery of DOX from PCL scaffolds reduced the incidence of DOX-related cardiotoxicity of mice compared to systemic administration. In addition, the combination of bioactive peptide (P24)-loaded biomaterials with DOX significantly minimized the detrimental effect of DOX on local bone regeneration of the cranial defects in rats.

In addition to the above-described cytotoxic drugs, biological response modifiers have been utilized to render bone substitutes therapeutically active for local anticancer therapy [86]. CD40 is a type I membrane glycoprotein normally expressed in B cells and dendritic cells, and the CD40/CD40L axis signals as a critical co-stimulatory pathway to facilitate antigen-presenting cell (APC) activation and cytotoxic T lymphocyte-mediated immunity against cancer cells. Since metastatic bone tumor cells (MDA-MB-231) highly express CD40, CD40-loaded poly(L-lactide) (PLLA) scaffolds induced apoptosis of MDA-MB-231 cells *in vitro*. In subcutaneous tumor models, the tumor volume treated with CD40-loaded biomaterials was 10-fold smaller as compared to tumors treated with antibody-free biomaterial. More importantly, CD40 antibody did not affect the proliferation of pre-osteoblast cells *in vitro*.

Since anticancer agents are heavily investigated for systemic treatment of bone tumors, they have a reliable therapeutic profile, which simplifies regulatory approval and enhances the translational potential.

In future, more *in vivo* preclinical studies on multifunctional bone substitute materials loaded with anticancer agents are required to verify their systemic biosafety and local anticancer efficacy in well-established bone tumor models.

4.5. Addition of agents to induce oxidative stress

Nanocatalytic cancer therapy has emerged as a promising approach with significant therapeutic efficacy against various cancers, while minimizing adverse effects on healthy tissues. This strategy capitalizes on the intrinsic acidic microenvironment prevalent in malignant tumors, characterized by elevated levels of hydrogen peroxide (H_2O_2) in tumor cells compared to the normal cells [87]. H_2O_2, one of the most representative reactive oxygen species (ROS), can undergo Fenton or Fenton-like chemical reactions and act as the reactant to be transformed into harmful ROS such as hydroxyl radicals (•OH) to target and eliminate cancer cells [88,89]. Furthermore, the acidic tumor environment can synergistically stimulate the excessive endogenous H_2O_2 to transfer into •OH to inhibit tumor growth. Considering those benefit, catalytically active agents have been combined with regenerative biomaterials and investigated for their therapeutic efficacy against malignant bone tumors (Table 3).

Typical catalytic Fenton reaction is the introduction of iron (Fe^{2+} and/or Fe^{3+}) ions into H_2O_2 to induce the transformation of highly toxic •OH. Therefore, Fe-based materials including single atomic Fe and Fe-based nanoparticles are the main agents utilized for induction of oxidative stress [90]. Zhang et al. reported ultrasound (US) – activatable semiconducting polymer nanoinducers ($ASPN_{FP}$) containing Fe_3O_4 nanoparticles as the ferroptosis inducers and plasma amine oxidase (PAO)-stabilized semiconducting polymer nanoparticles (SPN_P) encapsulated in singlet oxygen ($^1O_2$)-responsive nanocarriers for malignant bone tumor therapy [91]. Upon US irradiation, SPN_P in the $ASPN_{FP}$ generated $^1O_2$, and Fe_3O_4 nanoparticles were precisely released to trigger ferroptosis. The ROS fluorescence intensity in the $ASPN_{FP}$ + US group was 6.1-fold higher than those in the $ASPN_{FP}$ group. In an osteosarcoma metastasis mouse model, the $ASPN_{FP}$ + US treatment significantly suppressed tumor growth by 93.7%, and the relative tumor volume of the $ASPN_{FP}$ + US group was 0.5 which was much lower than the other groups ranged from 5.2 to 9.8. More importantly, the tibia in the $ASPN_{FP}$ + US group had the highest integrity, and the number of metastatic tumor nodules in the mice after $ASPN_{FP}$ + US treatment was significantly reduced compared to other groups.

One limitation hampering tumor-therapeutic efficiency of nanocatalytic cancer therapy is that the level of intracellular H_2O_2 in tumor cells is too low to generate sufficient •OH in the Fenton reaction to eliminate the tumor cells. Local reaction temperature is an important impact factor in the Fenton reaction, and high reaction temperature can enhance the production efficiency of •OH. To address this limitation,

Table 3
Bifunctional biomaterials fabricated by incorporation of oxidative stress-inducing agents.

Building block materials	Oxidative stress-inducing agent	Fabrication method	Local delivery form	*In vitro* therapeutic efficiency	Osteogenesis or biocompatibility assessments	*In vivo* bone tumor model	Initial tumor volume and *in vivo* therapeutic efficacy	Ref.
Bioactive glass	Single-atom iron catalysts (FeSAC)	Adsorption	3D-printed scaffold	Cell viability of Saos-2 cells decreased to 19.37%, 10.93% and 4.66% in $FeSAC_{1000}$-BG scaffold group under 0.5, 1.0 and 1.5 W cm^{-2} laser power density	Promoted the proliferation of hBMSCs; Upregulated the expression of COL 1, BMP-2, OCN and Runx2; Promoted bone defect repair in rats for the FeSAC-BG scaffold group	1×10^8 Saos-2 cells - subcutaneous tumor model; Balb/c mice	100 mm^3; Tumor volume decreased from 100 mm^3 to 0 mm^3 after 4 days in the FeSAC-BG + NIR group	[90]
Semiconducting polymer nanoparticles	Fe_3O_4 nanoparticles	Film-dispersion and hydration-sonication method	Nanoparticles	80.3% of morality rate on 4T1 cells in $ASPN_{FP}$ + US group	Lowest extent of tibia destruction, and no obvious lesions in kidney, spleen, and heart for $ASPN_{FP}$ + US group	2×10^6 4T1 cells - orthotopic bone tumor model in tibia	Relative tumor volume decreased to 0.5 in $ASPN_{FP}$ + US group	[91]
Akermanite (AKT, $Ca_2MgSi_2O_7$)	Fe_3O_4 nanoparticles and CaO_2 nanoparticles	Adsorption	3D-printed scaffold	All MNNG/HOS cells were eliminated in AKT-Fe_3O_4-CaO_2-AMF group	Promoted the proliferation of BMSCs; Upregulated the expression of ALP, BMP2, OCN, RUNX2, and COL1; Promoted new bone formation of cranial defect in rats in AKT-Fe_3O_4-CaO_2 group	2×10^6 MNNG/HOS cells - subcutaneous tumor model in mice; Balb/c mice	200 mm^3; 91.4% of inhibition efficacy in AKT-Fe_3O_4-CaO_2-AMF group	[92]
$CaSiO_3$	Fe	3D printing	3D-printed scaffold	91.4% of mortality rate on Saos-2 cells in 30CS group after 15 min irradiation	Promoted the proliferation of rBMSCs; Upregulated the expression of COL 1, OCN, Runx2 and BMP-2 of rBMSCs *in vitro*	5×10^6 Saos-2 cells - subcutaneous tumor model in mice	200 mm^3; Relative tumor volume decreased to less than 1 in the 30CS + ROS + laser group	[93]
Borosilicate	Cu^{2+} and Mn^{3+} ions	Sol-gel soft template method	Nanoparticles	Significant inhibitory effects on 143B cells	Significantly promoted proliferation of rBMSCs; Improved ALP activity and upregulated expression of BMP2, COL1A1 and RUNX2 of rBMSCs *in vitro*; Promoted bone regeneration and blood vessel formation *in vivo*	1×10^7 cells/mL 143B cells - subcutaneous bone tumor model; Balb/c mice	100–120 mm^3; Relative tumor volume decreased to around 1.3 in BSNs-Cu, BSNs-Mn and BSNs-Cu-Mn groups compared to around 2.3 in the control group	[94]

H_2O_2 supplier and photothermal agents are used to combine with biomaterials to enhance the •OH production, and synergistically improve the ultimate therapeutic efficacy [92]. For instance, a composite scaffold containing different amounts of Fe and $CaSiO_3$ (Fe-$CaSiO_3$) was developed, leading to a significant increase in the production efficiency of •OH upon exposure to near-infrared (NIR) irradiation (0.6 W/cm^2) [93]. The photothermal temperature of 30CS scaffold (wt%: 30% $CaSiO_3$ and 70% Fe) increased to 50 °C within 10 min, and the mortality rate of osteosarcoma cells increased to 91.4% after 15 min laser exposure *in vitro*. *In vivo* anticancer evaluation showed that the volume of the tumor tissue in the 30CS scaffold groups without irradiation was obviously smaller than that in the $CaSiO_3$ and $CaSiO_3$ + laser groups, and the 30CS scaffold + laser group exhibited the most effective tumor cell killing capacity. This indicated that the release of Fe and the photothermal agents synergistically enhanced therapeutic outcomes.

In addition to the mostly explored Fe-based Fenton nanoagents, other metal elements, such as Mn, Co, Cu and Ag, have shown promise as the Fenton-reaction catalysts. Cu-Mn-doped borosilicate (BS) nanoparticles killed osteosarcoma cells by significantly increasing the level of intracellular ROS [94]. Moreover, tumor growth was significantly slower in the mice treated with Cu-Mn-doped nanoparticles compared to the drastic increase of tumor volume in the mice treated with saline, and the incorporation Cu and Mn even promoted bone regeneration in lateral epicondyle defects in rats.

4.6. Addition of agents to induce local hyperthermia

Hyperthermic treatment of tumors by means of local temperature elevation is one of the oldest anticancer therapies, which has been applied since the 19th century [95], and it still is a widely used clinical therapy for treating cancers [96]. Usually, temperatures applied during hyperthermic treatment range between 41 and 46 °C. Within this temperature range, healthy cells do not undergo irreversible damage, while the nuclear synthesis in malignant cells is irreversibly inhibited which permanently destroys tumor cells because of the heat sensitivity [97]. In view of this, hyperthermia has been exploited in the design of bone substitute biomaterials with anticancer efficacy for treatment of malignant bone tumors.

Hyperthermic treatment is induced by photothermal agents: i) generating heat from NIR light, or ii) magnetothermal agents generating heat from alternating magnetic fields (AMF) to eradicate tumor cells. Therefore, the combination of biomaterials with either photothermal or magnetothermal agents can endow biomaterials with local hyperthermic ability. Photothermal strategies convert NIR light to local heat to ablate tumor cells in a minimally invasive manner due to precise control of laser irradiation conditions, which effectively minimizes undesired side effects of killing non-target cells. NIR-absorbing materials generally include organic agents (e.g. polydopamine, polyaniline, and cyanine dyes) [98,99], inorganic agents (e.g. carbon-based nano-systems, metal-based materials, and nonmetal materials), and transition metal elements (Table 4).

Polydopamine (PDA) is a representative organic material widely used as a photothermal agent in biomedical research owing to its excellent biocompatibility and biodegradability [100]. PDA was assembled onto 3D-printed biomaterials via soaking in the form of nanolayers and nanoparticles [101–103], and their exothermic temperatures increased to 42–94 °C upon 808 nm laser irradiation (0.34–1 W/cm^2). This photothermal temperature was sufficient to kill osteosarcoma cells, leading to more than 97.4% mortality *in vitro*. Moreover, when anticancer drug cisplatin was loaded on PDA-modified biomaterials, its release was stimulated by the temperature elevation as compared to PDA-free biomaterials, resulting in synergistic elimination of tumor cells. In subcutaneous tumor-bearing models, implantation of PDA-modified biomaterials increased temperatures of tumors to 52–60 °C with NIR laser irradiations (0.38–1.5 W/cm^2), which drastically reduced the average tumor weight and size. For successful treatment of bone defects after tumor resection, it is crucial that the bone-forming ability of the implanted scaffold is not affected by hyperthermia treatment. Therefore, these PDA-modified biomaterials were implanted into well-established bone defect models (e.g. skull and femoral defects) to assess their bone-forming activities, and the *in vivo* results demonstrated that bone regenerative capacities of PDA-modified biomaterials were not affected by short-time NIR irradiation.

Among various types of inorganic biomaterials, carbon-based materials are widely used in research as photothermal agents for hyperthermic treatment [104,105]. Carbon-based nanomaterials are considered particularly attractive compared to common inorganic materials due to their extremely high surface area [106,107]. Graphene and its derivatives such as graphene oxide (GO) are the most representative carbon-based nanomaterials, which have been combined with 3D-printed bioceramic scaffolds for bone tumor therapy and bone regeneration [108,109]. Upon 880 nm NIR irradiation (0.36–4.6 W/cm^2), the photothermal temperature in GO-loaded scaffolds increased to 50–64.8 °C, and the viability of osteosarcoma cells and metastatic breast tumor cells significantly decreased by 92.6% after 30 min laser exposure *in vitro*. The *in vivo* photothermal properties of the GO-loaded scaffolds were evaluated in subcutaneous osteosarcoma/-metastatic breast tumor-bearing mice models, and the temperatures at the tumor interior increased to over 50 °C. As a result, the tumor volumes in mice treated with GO-loaded scaffolds and laser irradiation significantly decreased. GO-loaded scaffolds without NIR irradiation were shown to promote bone regeneration, but it remains to be confirmed whether GO-loaded scaffolds can promote bone regeneration after NIR irradiation. Since high concentrations of GO are toxic to healthy cells, HA nanoparticles were incorporated into GO-loaded bioceramic scaffolds to alleviate this undesired side effect [110]. The results showed that *in vitro* toxic effects of GO declined with increasing amount of HA nanoparticles, and GO retained excellent NIR absorption abilities. More importantly, the *in vivo* photothermal effects against bone tumor and bone regenerative capacities of those scaffolds were not affected by HA incorporation.

Recently, ultrathin MXene nanosheets (a new class of 2D materials where “M” symbolizes transition metal atoms, “X” means carbon or nitrogen, and “ene” suffix deriving from “graphene” represents the materials with ultrathin 2D structure) have been explored for hyperthermic treatment of malignant bone tumors due to their high photothermal-conversion efficiency upon NIR irradiation [111,112]. 2D niobium carbide (Nb_2C) MXene has been explored for hyperthermic treatment of bone tumors, and the scaffolds loaded with Nb_2C MXene showed intrinsic photoresponse in the NIR-II (1064-nm laser) biological window, which led to high tissue-penetrating depth and effective killing of bone cancer cells *in vitro*. Moreover, *in vivo* antitumor assessment in subcutaneous osteosarcoma models showed that tumors were completely ablated, and the average survival time of tumor-bearing mice treated with Nb_2C MXene loaded scaffolds was significantly prolonged. In rat calvarial defect models, more newly formed bone and newborn vessels were observed in the defects treated with MXene-loaded scaffolds. Additionally, 2D MXene has been solely used as local carrier of therapeutic molecules (e.g. nitric oxide (NO) and immune adjuvants (R837)) to perform the combined therapy against bone tumors, and achieved synergistic effects on tumor elimination [113,114].

Metal-based materials including pure metal and metal-based compounds are a prominent category of photothermal agents for hyperthermic treatment of bone tumors [115]. For example, gold nano-materials have strong NIR laser absorption and excellent photothermal conversion efficiency in humans. These attractive features render gold nano-materials highly promising as photothermal agents for tumor ablation, which has resulted in clinical translation [116]. The temperature of gold nanorod-loaded hybrid hydrogels increased to 57.6 °C with a heating penetration depth of 3.7 mm in bone upon NIR irradiation (0.08–0.99 W/cm^2) [117], which killed over 98% of

Table 4
Bifunctional biomaterials functionalized with hyperthermic properties.

Building block materials	Photothermal agent	Fabrication method	Local delivery form	Maximum temperature	*In vitro* therapeutic efficiency	Osteogenesis or biocompatibility assessments	*In vivo* bone tumor model	Initial tumor volume and *in vivo* therapeutic efficacy	Ref.
PLGA	Curcumin	Emulsion/evaporation	Hydrogel	~51 °C in air	Cell viability of K7M2wt osteosarcoma cells reduced to 55.8% and 23.9% for IR820 gel + laser and Cur-MP/IR820 gel + laser, respectively	No negative effects on proliferation of NIH3T3 cells; Activation of ALP in BMSCs and a higher amount of calcium nodules *in vitro*	~2 mm^3 tumor mass (K7M2wt tumor tissue plagues) - in situ bone tumor model; Balb/c mice	Majority of the tumor mass (total tumor volume of around 1400 mm^3) was ablated in the IR820 gel + laser and Cur-MP/IR820 gel + laser groups	[98]
Bioactive glass	Chlorin e6	Evaporation-induced self-assembly	Sintered scaffold	83 °C in air and 53.8 °C in PBS for 5Mn-MBG; 62.6 °C in air and 43.4 °C in PBS for 2Mn-MBG	Cell viability of MG63 cells decreased to 77.7%, 60.5% and 21.1% in 5Mn-MBG/Ce6+PTT, 5Mn-MBG/Ce6+PDT and 5Mn-MBG/Ce6+PTT + PDT groups, respectively	No obvious side effects on bone regeneration of the critical-sized cylindrical bone defects in rats and rabbits	2.0×10^5 LM8 osteosarcoma cells - subcutaneous tumor model in mice	4 mm in diameter; Relative tumor volume decreased to 0 in the 5Mn-MBG/Ce6+PTT + PDT group	[99]
Magnesium oxide nanoparticles	Polydopamine	Oxidation and self-polymerization/ Dispersion polymerization	3D scaffold	~47.5 °C	Apoptotic rate of 143B cells increased to 91.8% in the 10NP/CMP@PAM + NIR group	No negative effects on the proliferation of MC3T3-E; Upregulated the expression of Runx 2, OSX and OCN; Promoted the new bone formation of the calvarial defect in rats in the 5NP/CMP@PAM + NIR group	2×10^7 143B cells - subcutaneous tumor model; Balb/c mice	100 mm^3; Tumor suppression rate reached 100% in the 5NP/CMP@PAM + NIR group	[100]
CaP ($Ca_7Si_2P_2O_{16}$)	Polydopamine	Adsorption	3D-printed scaffold	~92 °C in air and ~50 °C in PBS; 7.5 mm	~97.4% and ~99.2% of mortality for MDA-MB-231 cells and Saos2 cells	No negative effects on the proliferation of rBMSCs; Stimulated bone regeneration of the femoral bone defect in rabbits	1×10^6 MDA-MB-231-luc cells - subcutaneous tumor model in mice	200 mm^3; Tumor weight decreased from around 1.5 to 0.2g in DOPA-BC + NIR laser group	[101]
HA	Polydopamine	Schiff base reaction	Nanoparticles	~42 °C	Significant cytotoxic effects on 4T1 cells	No negative effects on proliferation of BMSCs; Promoted ALP activity of BMSCs; PHA-DDP promoted bone regeneration of defects in rabbits compared to blanks	1×10^6 4T1 cells - subcutaneous tumor model in mice	200 mm^3; Tumor volume decreased to 75 mm^3 in the OSA-CS-PHA-DDP + NIR group	[102]
Polylactic-co-glycolic acid (PLGA) and tricalcium phosphate (TCP)	Polydopamine	Freeze-drying	3D-printed scaffold	~94 °C in aqueous solutions	Significant cytostatic effects on 4T1 cells in the FeMg-NPs + Laser group	Promoted the proliferation of BMSCs (Mg^{2+} concentrations: $5–10 \times 10^{-3}$ M); Upregulated the expression of OPN, Runx 2 and Col-1; Promoted new bone formation of calvarial defects in rats for FeMg- scaffold group	4T1 cells - subcutaneous tumor model; Balb/c mice	Relative tumor volume significantly decreased, and tumor weight deceased to 0.1g in FeMg-scaffold + Laser group	[103]
β-TCP	Carbon aerogel	Adsorption	3D-printed discs	~74 °C in PBS	Significant inhibitory effects on MNNG/HOS cells in β-TCP-C-laser group	Promoted the proliferation of BMSCs; Upregulated the expression of ALP, BMP2, OCN and OPN in BMSCs; Produced more bone tissue in the β-TCP-C-laser group in rats	1×10^6 MNNG/HOS cells - subcutaneous tumor model; Balb/c mice	200 mm^3; 81.85% of tumor suppression rate in β-TCP-C-laser group	[104]
Chitosan and nanohydroxyapatite	Zero-dimensional carbon dots	Freeze drying	3D scaffold	41.8–52.6 °C in PBS	Almost all UMR-106 cells died after 10 min	CS/nHA/CD scaffolds upregulated the expression of ALP, COL-1 and OCN of	5×10^6 UMR-106 cells - subcutaneous	7~10 mm in diameter; Tumor volume decreased to	[105]

(*continued on next page*)

Table 4 (*continued*)

Building block materials	Photothermal agent	Fabrication method	Local delivery form	Maximum temperature	*In vitro* therapeutic efficiency	Osteogenesis or biocompatibility assessments	*In vivo* bone tumor model	Initial tumor volume and *in vivo* therapeutic efficacy	Ref.
					irradiation in the CS/nHA/CD + NIR group	rBMSCs *in vitro*, and promoted new bone tissue, collagen and vessel formation of the bone defect in rats	tumor model; Balb/c mice	around 0 mm^3 in CS/nHA/CD3+NIR group	
Larnite (silicone resin)	Porous free carbon ($CaCO_3$ fillers)	3D printing	3D-printed scaffold	61–63 °C in air and 46–48 °C in PBS	Cell viability of MNNG/HOS cells on larnite/C-3 scaffolds decreased to 70%, 48%, 27% and 5% at a power intensity of 0.5, 0.75, 1 and 1.25 W/cm^2, respectively	Promoted the infiltration and proliferation of rBMSCs; Upregulated the expression of ALP, OCN and Runx-2 of rBMSCs; more newly formed bone observed in calvarial defect of rats in the larnite/C-3 scaffold group	5.0×10^4 MNNG/HOS cells - subcutaneous tumor model	200 mm^3; Relative tumor volume decreased to 0 in the larnite/C-3+NIR group	[106]
Akermanite	Borocarbonitrides	Dip coating	3D-printed scaffold	85.7–109 °C in air and 50.7–61.2 °C in PBS	Cell viability of MNNG/HOS cells decreased to 11% in the 5BCN@AKT + laser group	Promoted the proliferation of hBMSCs; Upregulated the expression of BMP2, AL, COL 1, BSP, OPN and OCN of hBMSCs; Promoted new bone formation of femoral defect in rabbits	1.5×10^6 MNNG/HOS cells - subcutaneous tumor model	200 mm^3; Relative tumor volume decreased to 0 in the 5BCN@AKT + laser group	[107]
β-TCP	Graphene oxide	Adsorption	3D-printed scaffold	71–85 °C in air and 39–45 °C in PBS	Cell viability of MG-63 in the GO-TCP scaffold group decreased by 92.6% after 30 min irradiation	Improved ALP activity and upregulated the expression of RUNX2, OCN and BSP of rBMSCs *in vitro*; Promoted the bone regeneration of the calvarial defect in rabbits	5×10^6 Saos-2 tumor cells - subcutaneous tumor model; Balb/c mice	300 mm^3; Tumor volume and size drastically decreased, and tumor cell necrotic rate of 83.28% in GO-TCP scaffolds	[108]
Chitosan and $CePO_4$ nanorods	GO nanosheets	Freeze-drying	3D scaffold	~64.8 °C in air	Significant cytotoxic effects on MDA-MB-231 cells in $CePO_4$/CS/GO group	Promoted the proliferation of hBMSCs and MC3T3-E1 cells; Upregulated the expression of ALP, BMP-2, OCN and RUNX2; Accelerated new bone formation of the calvaria defect in rats in $CePO_4$/CS and $CePO_4$/CS/GO groups	5×10^7 MDA-MB-231 cells - subcutaneous tumor model in mice	6 mm in diameter; Relative tumor volume decreased from 1 to around 0.5 in the $CePO_4$/CS/GO scaffold group	[109]
Chitosan	Graphene oxide nanoparticles	Adsorption	3D scaffold	37.7–61.3 °C in PBS	52.3% of apoptosis rate and 17.6% of necrosis rate on HOS cells in 30% nHA/GO	Promoted the proliferation of hBMSCs and MC3T3-E1 cells and upregulated the expression of ALP, RUNX2 Col 1 and OCN of hBMSCs *in vitro*; GO/CS and nHA/GO/CS promoted new bone formation in cranial defects in rats	1×10^7 HOS cells - orthotopic bone tumor model in hip; Balb/c-nude mice	8 mm in diameter; Relative tumor volume decreased from around 6 to less than 1 in GO/CS + laser and nHA/GO/CS + laser groups	[110]
Bioactive glass	Ti_3C_2 MXenes	Adsorption	3D-printed scaffold	40–65 °C in air and 42–58 °C in PBS in 1.0 TBGS group	Cell viability of Saos-2 cells decreased to less than 40% in TBGS + laser group	Promoted the proliferation of hBMSCs *in vitro*; Upregulated the expression of COL 1, RUNX2, OCN and OPN of hBMSCs in TBGS group; Promoted new bone formation in cranial defects of rats	4×10^6 Saos-2 cells - subcutaneous tumor model; BALB/c nude mice	120 mm^3; Tumor volume decreased from around 500 mm^3 to 0 mm^3 in TBGS + NIR group	[111]
Bioactive glass	2D niobium carbide (Nb_2C) MXene	Adsorption	3D-printed scaffold	~56 °C in PBS	Cell viability of Saos-2 cells decreased to less than 38% in NBGS + NIR group	Promoted the proliferation of hBMSCs; Upregulated expression of COL 1, Runx2, OCN and OPN; Facilitated the	1×10^5 Saos-2 cells - subcutaneous	180 mm^3; Tumor volume decreased from 1250 to around	[112]

(*continued on next page*)

Table 4 (*continued*)

Building block materials	Photothermal agent	Fabrication method	Local delivery form	Maximum temperature	*In vitro* therapeutic efficiency	Osteogenesis or biocompatibility assessments	*In vivo* bone tumor model	Initial tumor volume and *in vivo* therapeutic efficacy	Ref.
						repair of calvarial defects of rats in NBGS + NIR group	tumor model; BALB/c nude mice	0 cm^3 in NBGS + NIR group	
Bioactive glass	Nb_2C MXene	Deposition	3D-printed scaffold	38–60 °C in air	Cell viability of Saos-2 cells decreased to 25–35% after 10 min irradiation	No significant cytotoxicity on hBMSCs; Upregulated the expression of COL1, OCN, BMP-2 and RUNX2; Promoted new osseous tissue formation in calvarial defects in rats	4×10^6 Saos-2 cells - subcutaneous tumor model; BALB/c nude mice	120 mm^3; Tumor volume decreased to 0 mm^3 in MBGS + NIR- II and MBS + NIR- II groups	[113]
Bioactive glass	Nb_2C MXene	Adsorption	3D-printed scaffold	~71.1 °C in air	Significant inhibitory effects on the proliferation of MDA-MD-231 and MCF7	Accelerated bone regeneration in calvarial defects in rats for the BG@NbSiR group	1×10^6 4T1 cells - orthotopic distant metastasis model in mice	65 mm^3; Tumor volume remained around 0 mm^3 in the PTT + anti-PD-L1 group	[114]
PLGA	Mg particles	Low-temperature rapid-prototyping technology	3D-printed scaffold	~140.65 °C in air and ~43.57 °C in PBS	Apoptotic rate of Saos-2 cells increased to 94.6% in P10 M + NIR group	Promote the osteogenic differentiation of MC3T3-E1 cells; Upregulated the expression of BMP2, BSP, OCN and OPN; Promoted new bone formation in the bone defect region in rats	2×10^7 Saos-2 tumor cells - subcutaneous tumor model; BALB/c mice	150 mm^3; Relative tumor volume decreased to around 0 in P10 M + NIR group	[115]
GelMA/CSMA hydrogel	Gold nanorods	Photopolymerization	3D scaffold	35.0–57.6 °C in air	Cell viability of K7M2wt cells decreased to 99.3%, 73.0% and 1.2% in 0.08, 0.56, 0.99 W/cm^2 groups	No negative effects on the spread and proliferation of MSCs; Promoted osteogenic differentiation of MSCs *in vitro*; Promoted bone formation in tibial bone defects in the surgery + hydrogel + PTT group	1.0×10^6 K7M2wt cells - ectopic tumor harvest - orthotopic tibia tumor; BALB/c mice	~5 mm in diameter; Tumor volume remained around 0 mm^3 in the surgery + hydrogel + PTT group	[117]
Bioactive glass	Copper	Diels–Alder (DA) reaction	3D-printed scaffold	56–58.8 °C in air and 52.8–57.4 °C in PBS	Cell viability of K7M2-WT cells decreased to 28.9%, 23.6% and 19.1% in SA/PEG-2CuBGM, SA/PEG-3CuBGM and SA/PEG-4CuBGM groups	Promoted the proliferation of mBMSCs in SA/PEG-CuBGM group; Upregulated the expression of ALP, OPN, COL1 and RUNX2; Promoted bone formation in femoral defects in rats in SA/PEG-CuBGM group	5×10^6 K7M2-WT cells - subcutaneous tumor model; BALB/c mice	150 mm^3; Relative tumor volume decreased to around 0 in the SA/PEG-3CuBGM + NIR group	[118]
Bioactive glass	Elements (Cu, Fe, Mn and Co)	Sol-gel method	3D-printed scaffold	60–90 °C in air and 44–52 °C in PBS	Cell viability of Saos-2 cells decreased to 1.2%, 17.6%, 37.4% and 43.1% for 5Cu-BGC, 5Fe-BGC, 5Mn-BGC and Co-BGC groups, respectively	No negative effects on the proliferation of rBMSCs in the 5Fe-BGC and 5Mn-BGC groups; Significant cytostatic effects on rBMSCs in the 5Cu-BGC and 5Co-BGC groups	5×10^6 Saos-2 cells - subcutaneous tumor model in mice	114 mm^3; Tumor cell necrotic rate increased to 94.9%, 90% and 72% for the 5Cu-BGC + laser, 5Fe-BGC + laser and 5Mn-BGC + laser groups, respectively	[119]
Bioactive glass	$CuFeSe_2$ nanocrystals	Solvothermal method	3D-printed scaffold	80–143 °C in air and 33–72 °C in PBS	Significant cytostatic effects on Saos-2 cells in BG-5CFS scaffold group	Promoted the proliferation of rBMSCs; Upregulated expression of OCN and OPN; Promoted new bone formation in the femoral defect of rabbits	5×10^6 Saos-2 cells - subcutaneous tumor model in mice	8 mm in diameter; Relative tumor volume decreased to around 0.5 in BG-5CFS scaffold group	[120]
Bioglass	Black phosphorus (BP) nanosheets	Surface modification	3D-printed scaffold	32.4–68.7 °C	Significant inhibitory effects on Saos-2 cells in the BP-BG NIR group	Upregulated the expression of OPN, OCN, ALP, COL 1 and RUNX2 of hBMSCs and	5×10^6 Saos-2 cells - subcutaneous	200 mm^3; Relative tumor volume	[121]

(*continued on next page*)

Table 4 (*continued*)

Building block materials	Photothermal agent	Fabrication method	Local delivery form	Maximum temperature	*In vitro* therapeutic efficiency	Osteogenesis or biocompatibility assessments	*In vivo* bone tumor model	Initial tumor volume and *in vivo* therapeutic efficacy	Ref.
						accelerated their osteogenic differentiation *in vitro*	tumor model; Balb/c nude mice	decreased to 0 in the BP-BG NIR group	
Akermanite	MoS_2	Hydrothermal method	3D-printed scaffold	107–120 °C in air and 38–55 °C in PBS	Cell viability decreased to 26% for Saos-2 cells and 23% for MDA-MB-231 cells in the MS-AKT + Laser group	Upregulated the expression of RUNX2, OCN, OPN and ALP of rBMSCs; Promoted new bone formation in femoral defects in rabbits	5×10^6 Saos-2 tumor cells - subcutaneous tumor model; Balb/c mice	10 mm in diameter; Tumors disappeared by day 14, and 89% of tumor cell necrotic rate in the MS-AKT + laser group	[122]
$CaCO_3$ and PCL	Egyptian blue ($CaCuSi_4O_{10}$) nanosheets	Solid-state reaction	3D-printed scaffold	33–61 °C	Cell viability of 143B and HOS cells decreased to less than 8% after 5 min laser irradiation	Upregulated the expression of RUNX2, OCN and BMP2; Promoted new bone formation in calvarial defect in rats for the CaPCu group	143B cells - subcutaneous tumor model; BALB/c mice	60 mm^3; Tumor volume decreased from 60 mm^3 to around 0 mm^3 in the CaPCu + NIR group	[123]
β-TCP	Cu-TCPP	*In-situ* growth method	3D-printed scaffold	84.58–108.18 °C in air and 42.04–55.07 °C in PBS	90% of mortality rate on LM8 osteosarcoma cells after 10 min irradiation in the 20Cu-TCPP-TCP group	Upregulated the expression of ALP, BMP2, OCN and RUNX2 in HBMSCs; Significantly enhanced the osteogenic and angiogenic differentiation of HBMSCs and HUVECs; Promoted the regeneration of new bone tissues in femoral defects in rabbits	7×10^6 Saos-2 cells - subcutaneous tumor model in mice	8 mm in diameter; Relative tumor volume decreased from around 5.7 to 0.5 in the 20Cu-TCPP-TCP + NIR group	[124]
Calcium phosphate cements (CPC)	Co-TCPP nanosheets	Physical mixing	Cement	71–95 °C in air and ~50 °C in PBS	Cell viability of MG-63 cells decreased to 3% in the 1% Co-TCPP/CPC + laser group	Promoted the proliferation of rBMSCs At low concentration of cobalt ions; Upregulated the expression of BMP2, OCN and RUNX 2; Promoted new bone formation in femoral defects in rabbits	2×10^5 LM8 cells - subcutaneous tumor model in mice	3 mm in diameter; Relative tumor volume decreased to around 0 in 1%Co-TCPP/CPC + laser group	[125]
PCL	Wesselsite ($SrCuSi_4O_{10}$) nanosheets	Physical mixing	3D-printed scaffold	~55 °C	Cell viability of Saos-2 cells decreased to less than 10% in the 4-SC/PCL group	No significant cytostatic effects on proliferation of rBMSCs and HUVECs; Upregulated the expression of OCN, BMP2 and RUNX2; Promoted new bone formation in calvarial defects in rats in the 4-SC/PCL scaffold group	1×10^7 Saos-2 cells - subcutaneous tumor model in mice	100 mm^3; Relative tumor volume decreased to around 0 in the 4-SC/PCL + NIR group	[126]
Akermanite	Fe_3S_4 microflowers	Hydrothermal process	3D-printed scaffold	~90 °C in air and ~55 °C in PBS	Cell viability of MG 63 decreased to 1.54% when temperature reached 52 °C	No negative effect on the proliferation of hBMSCs; Upregulated the expression of OCN, RUNX2 and BSP; Promoted new bone formation of femoral defects in rabbits for AKT and Fe_3S_4-AKT groups	2.0×10^5 LM-8 cells - subcutaneous tumor model in mice	300 mm^3; Tumor volume decreased to 0 mm^3 in the Fe_3S_4 -AKT + AMF group	[127]
Akermanite	Fe_3O_4 nanoparticles	Adsorption	3D-printed scaffold	~80 °C at pH 7.4 and ~60 °C at pH 6.0 in PBS	All MNNG/HOS cells died under AMF in AKT-Fe_3O_4-CaO_2 group	Negligible toxic impact on rBMSCs; Upregulated the expression of BMP2, OCN, RUNX2 and COL 1 in rBMSCs and promoted the adhesion and osteogenic differentiation of rBMSCs; Stimulated	2×10^6 MNNG/HOS cells - subcutaneous tumor model; Balb/c mice	200 mm^3; 15.8%, 45.3%, 63.2% and 91.4% inhibition efficacy in the AKT-Fe_3O_4, AKT-Fe_3O_4-CaO_2, AKT-Fe_3O_4-AMF and AKT-Fe_3O_4-	[130]

(*continued on next page*)

Table 4 (*continued*)

Building block materials	Photothermal agent	Fabrication method	Local delivery form	Maximum temperature	*In vitro* therapeutic efficiency	Osteogenesis or biocompatibility assessments	*In vivo* bone tumor model	Initial tumor volume and *in vivo* therapeutic efficacy	Ref.
						osteogenesis in cranial defects in rats		CaO_2-AMF groups, respectively	
Calcium silicate ($CaSiO_3$) and chitosan	$SrFe_{12}O_{19}$, doxorubicin	Freeze drying	Mesoporous scaffold	~55 °C in air	Moderate anti-proliferative impacts on MG-63 cells in MCSC 1:7/DOX and MCSC 1:3/DOX scaffolds	Promoted the proliferation of hBMSCs; Upregulated the expression of BMP-2, Smad and Runx2 of hBMSCs	5×10^6 MNNG osteosarcoma cells - subcutaneous tumor model in mice	Relative tumor volume decreased from around 3.0 to 0.5 in MCSC1:3/DOX-NIR group	[131]
Bioglass and chitosan	$SrFe_{12}O_{19}$ nanoparticles	Freeze drying	3D-printed scaffold	~46.3 °C	Time-dependent cytostatic effects on MG-63 cells in MBCS1:7 and MBCS 1:3 groups	Promoted the proliferation of hBMSCs; Upregulated expression of OCN, COL1, Runx2 and ALP of hBMSCs	5×10^6 MNNG tumor cells - subcutaneous tumor model in mice	300 mm^3; Tumor cell necrotic rate increased to 84.6% in the MBCS1:3/NIR group	[132]
α-tricalcium phosphate (α-TCP)/calcium sulfate cement (CSC)	Fe_3O_4/graphene oxide (GO) nanocomposites	Mixing	Biphasic bone cement	45–73 °C in air and 45–54 °C in PBS	Cell viability of 143B cells decreased to 48.6% after 24h	No negative effects on the adhesion and proliferation of rBMSCs; Promoted new bone tissue growth in cranial defect of rats	1×10^7 cells 143b cells - subcutaneous tumor model in mice	8 mm in diameter; Relative tumor volume decreased to less than 1 in the αC-10FG + AMF group	[133]

osteosarcoma cells *in vitro*. In an orthotopic osteosarcoma model of mice, the hybrid hydrogel was implanted after surgical resection of orthotopic osteosarcoma, which eradicated the residual tumor tissue and prevented further recurrence. In addition, NIR-responsive transition metal elements are more appropriate as photothermal energy converters for hyperthermic tumor therapy than other optical absorbers due to plasmonic characteristics, strong optical, and thermal stabilities [118]. For instance, several elements (e.g., Cu, Fe, Mn, Co) were doped either separately or collectively into 3D-printed BG scaffolds, and after laser irradiation (1 W/cm^2) of scaffolds containing multiple elements more than 95% of osteosarcoma cells on these doped scaffolds were killed *in vitro* [119]. Moreover, upon NIR irradiation with a laser density of 0.54 W/cm^2, scaffolds doped with single elements exhibited various photothermal anticancer effect following the trend: Cu-BGC > Fe-BGC > Mn-BGC > Co-BGC > BGC, which indicated that the photothermal effect depends on the specific element. *In vivo* anticancer assessment showed that Cu- and Fe-doped scaffolds resulted in tumor tissue necrosis rate of 94.9% and 90%, corresponding to superior photothermal anticancer performance compared to other elements.

Besides pure metals, metal-based compounds (e.g. 2D metal-based nanocrystals and nanosheets) have also gained interest as photothermal agents for hyperthermic treatment of bone tumors due to their high photothermal conversion, surface area, and photostability [120]. 2D nanosheets such as semiconductors [121,122], metal-based chalcogenides [123], and metal-organic framework (MOF) [124,125] possess flexible surface and high surface area, which can rapidly respond to external light and exhibit high photothermal conversion efficiency. Egyptian blue (EB, $CaCuSi_4O_{10}$) and strontium copper tetrasilicate ($SrCuSi_4O_{10}$, SC), which are representative copper-containing chalcogenides, have been reported to display excellent absorption in the NIR-II bio-window (1000–1350 nm) with superior penetration depths compared to irradiation by NIR-I lasers (650–1000 nm) [123]. Metal-based chalcogenides were used in combination with 3D-printed PCL scaffolds, and the exothermal temperature increased to over 45 °C upon 1064 nm laser irradiation (0.6 W/cm^2) within 5 min, leading to more than 90% mortality of osteosarcoma cells *in vitro* [126]. *In vivo* evaluation of antitumor effects showed that the tumor temperature rapidly raised to 53.4 °C upon irradiation of the scaffold with a laser, which resulted in complete tumor eradication vs. progressive tumor growth in controls. The aforementioned metal-based bifunctional biomaterials promoted proliferation of bone marrow stromal cells (BMSCs) and upregulated the osteogenic gene expression *in vitro*. Furthermore, *in vivo* evaluation of osteogenesis in bone defect models surprisingly demonstrated that the introduction of metal-based photothermal agents promoted new bone formation.

Different from NIR-absorbing materials, stimulation of magnetothermal agents by an AMF results in heating to locally induce hyperthermia [127]. Magnetothermal therapy generated by magnetic heating seeds deeply penetrates tissues and organs within the human body [128]. Moreover, magnetic fields can stimulate cell responses to control cell behaviors including cell proliferation and differentiation [129]. To date, nano-sized magnetite (Fe_3O_4) is the most popular type of magnetic heating seed for hyperthermic treatment due to its low activation energy, high temperature increase, chemical stability, and porous oxide structure. Fe_3O_4-loaded 3D-printed Akermanite (AKT, $Ca_2MgSi_2O_7$) scaffold was subjected to AMF irradiation (500 KHz; output current, 22 A; coil diameter, 10 cm), and its temperature increased to 90 °C within 1 min [130]. Sufficient hyperthermia and ·OH hydroxyl radical were produced to kill human osteosarcoma cells *in vitro*, and 91.4% of subcutaneous osteosarcomas were eradicated *in vivo*. In addition to Fe_3O_4 magnetite, selected ferrites have also been investigated as magnetic heating seeds for application of magnetic hyperthermia therapy [131,132].

However, the hyperthermic efficacy of Fe_3O_4 nanoparticles incorporated in biomaterials can be compromised by shielding and poor thermal conductivity of the surrounding biomaterial matrix. To

overcome this problem, GO and Fe_3O_4 nanoparticles were added together to biphasic bioceramic bone cement, resulting in heating curves rising up to 73 °C in air (48 KHz, +6000 and −6000 Oe at 300 K) [133]. Furthermore, this bone cement selectively killed osteosarcoma cells *in vitro*, and led to enhanced tumor tissue necrosis and less lung metastasis compared to the controls *in vivo*. Similar to the metal-based photothermal agents, magnetothermal agents hardly reduced adhesion and proliferation of BMSCs, upregulated the osteogenic genes of BMSCs *in vitro*, and accelerated new bone growth of bone defects *in vivo*.

5. Conclusion and future perspectives

With the development of image-guided surgery and progress of chemotherapeutic drug development and efficacy, the 5-year survival rate of bone tumors has significantly improved over the last years. However, high lethality due to local recurrence rates of malignant bone tumors remains a major clinical stumbling block toward effective bone tumor therapy. In view of the frequent use of bone substitutes to regenerate bone defects after tumor resection, different strategies for the design of bone substitutes with dual functionality to simultaneously stimulate bone regeneration and exert anti-tumor efficacy have been proposed. These strategies take advantage of local anti-tumor efficacy in the direct vicinity of the resected tumor tissue, which facilitates elimination of residual tumor cells and circumvents systemic chemotherapy associated with detrimental side effects.

Bifunctional bone substitutes for treatment of bone tumors can be therapeutically active based on i) intrinsic anti-tumor efficacy of specific biomaterials, ii) loading of bone substitutes with anticancer agents, iii) loading of bone substitute with oxidative stress-inducing agents, or iv) loading of bone substitutes with hyperthermic agents. The combined evidence of all *in vitro* studies suggests that these four strategies to develop bifunctional bone substitutes have the potential to render commonly used conventional bone substitute biomaterials therapeutically active against tumor cells. Moreover, most of the aforementioned studies provided *in vivo* evidence as well confirming that bifunctional bone substitutes can inhibit tumor growth in subcutaneous bone tumor models and promote new bone formation in bone defect models.

While initial progress in development and preclinical evaluation of bifunctional bone substitutes is encouraging, clinical translation of these novel biomaterials is still largely lacking (Fig. 4A). Several issues need to be addressed to expedite their clinical translation. The most important hurdle towards translation relates to the lack of suitable models to test both bone regenerative and anticancer efficacy simultaneously in a combined and reliable manner. Currently, the bone-regenerative capacity of bifunctional bone substitutes is evaluated in well-established bone defect models, which lack the presence of a bone tumor. In contrast, the anticancer efficacy of these bifunctional biomaterials is predominantly tested in non-osseous ectopic tumor models (e.g. at subcutaneous sites; Fig. 4B), which lack physiological and anatomical resemblance with bone and predictability for clinical efficacy.

Due to the presence of an immune system, orthotopic bone tumor models have been developed and used as *in vivo* testing model, but orthotopic bone tumor models can only be developed in immunodeficient mice. However, the volume of mouse bone is small, and after tumor preparation the tumor resection and subsequent filling of biomaterials are almost physically impossible. Although mice are isogenic, the individual sensitivity to tumor cells is still different, which can result in significant inter-individual differences in tumor volume after modeling. More importantly, bone tumors grow uncontrollably following tumor cell injections. If the timepoint of intervention is too late, tumors may be too large for surgical removal or may have already metastasized, scenarios which both have a detrimental impact on animal welfare.

Nevertheless, tumor ablation based on photothermal agent has progressed to the clinical trial phase for treatment of prostate cancers [116], but clinical evidence for their anticancer efficacy in the treatment of primary or metastatic bone tumor has not yet been obtained. In addition, bifunctional biomaterials are generally recognized as potent eliminators of tumor cells while simultaneously promoting bone healing, but the balance between their chemotherapeutic efficacy vs. dose-dependent local and systemic toxicity as well as long-term biosafety still needs to be confirmed in suitable bone tumor models before extensive clinical testing can be considered.

This review highlighted the most common strategies to design bifunctional biomaterials which can promote bone regeneration and simultaneously kill residual tumor cells after bone tumor resection. By exploiting the intrinsic anticancer efficacy of specific biomaterial components, adding anticancer agents, incorporating oxidative stress-inducing agents, and/or incorporating hyperthermia generators into appropriate bone substitute materials, optimized treatment strategies can be generated in future by multidisciplinary teams consisting of chemists, material scientists, pharmacists, oncologists, and surgeons to offer new therapeutic solutions for patients suffering from bone tumors.

CRediT authorship contribution statement

Zhule Wang: Conceptualization, Methodology, Investigation, Data curation, Writing - original draft, Writing - review & editing. **Ingrid CM van der Geest:** Conceptualization, Supervision. **Sander CG. Leeuwenburgh:** Conceptualization, Methodology, Supervision, Project administration, Writing - review & editing. **Jeroen JJP. van den Beucken:** Conceptualization, Methodology, Supervision, Project administration, Writing - review & editing.

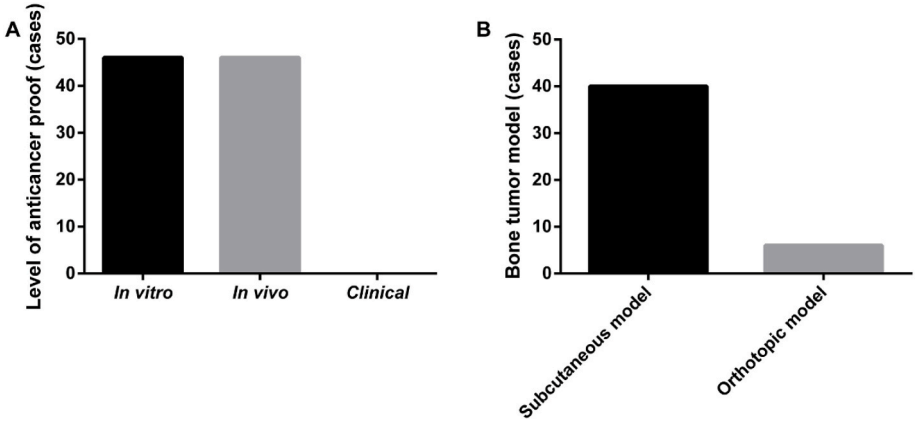

Fig. 4. Literature overview of types of preclinical studies confirming anticancer efficacy of bifunctional bone substitute materials. (A) Numbers of studies reporting anticancer efficacy of bifunctional bone substitute materials based on *in vitro* (cell culture), *in vivo* (animal), or clinical (human patient) studies. (B) Numbers of studies using *in vivo* bone tumor models at separate sites (subcutaneous vs. orthotopic).

Declaration of competing interest

The authors declare that they have no known competing financial interests or personal relationships that could have appeared to influence the work reported in this paper.

Data availability

No data was used for the research described in the article.

Acknowledgments

ZL.W. is funded by China Scholarship Council (Project No. 201908510125).

References

[1] R. Coleman, P. Hadji, J.J. Body, D. Santini, E. Chow, E. Terpos, et al., Bone health in cancer: ESMO clinical practice guidelines, Ann. Oncol. 31 (12) (2020) 1650–1663, https://doi.org/10.1016/j.annonc.2020.07.019.
[2] L.A. Torre, R.L. Siegel, E.M. Ward, A. Jemal, Global cancer incidence and mortality rates and trends–an update, Cancer Epidemiol. Biomarkers Prev. 25 (1) (2016) 16–27, https://doi.org/10.1158/1055-9965.EPI-15-0578.
[3] K.D. Miller, L. Nogueira, A.B. Mariotto, J.H. Rowland, K.R. Yabroff, C.M. Alfano, et al., Cancer treatment and survivorship statistics, 2019, CA A Cancer J. Clin. 69 (5) (2019) 363–385, https://doi.org/10.3322/caac.21565.
[4] F. Macedo, K. Ladeira, F. Pinho, N. Saraiva, N. Bonito, L. Pinto, et al., Bone metastases: an overview, Onco Rev. 11 (1) (2017) 321, https://doi.org/10.4081/oncol.2017.321.
[5] T. Tarver, Cancer facts & figures 2012. American cancer society (ACS), J Cons Hlth Internet 16 (3) (2012) 366–367, https://doi.org/10.1080/15398285.2012.701177.
[6] O. Sartor, J.S. de Bono, Metastatic prostate cancer, N. Engl. J. Med. 378 (7) (2018) 645–657, https://doi.org/10.1056/NEJMra1701695.
[7] J.F. Huang, J. Shen, X. Li, R. Rengan, N. Silvestris, M. Wang, et al., Incidence of patients with bone metastases at diagnosis of solid tumors in adults: a large population-based study, Ann. Transl. Med. 8 (7) (2020) 482, https://doi.org/10.21037/atm.2020.03.55.
[8] W. Liu, J. Wu, Lung cancer with bone metastases in the United States: an analysis from the surveillance, epidemiologic, and end results database, Clin. EEG Neurosci. 35 (8) (2018) 753–761, https://doi.org/10.1007/s10585-018-9943-5.
[9] B.A. Gartrell, F. Saad, Managing bone metastases and reducing skeletal related events in prostate cancer, Nat. Rev. Clin. Oncol. 11 (6) (2014) 335–345, https://doi.org/10.1038/nrclinonc.2014.70.
[10] S. Falk, A.H. Dickenson, Pain and nociception: mechanisms of cancer-induced bone pain, J. Clin. Oncol. 32 (16) (2014) 1647–1654, https://doi.org/10.1200/JCO.2013.51.7219.
[11] M.J. Goblirsch, P.P. Zwolak, D.R. Clohisy, Biology of bone cancer pain, Clin. Cancer Res. 12 (20 Pt 2) (2006), https://doi.org/10.1158/1078-0432.CCR-06-0682, 6231s-5s.
[12] M.R. Dionisio, A. Mansinho, C. Abreu, J. Cavaco-Silva, S. Casimiro, L. Costa, Clinical and translational pharmacology of drugs for the prevention and treatment of bone metastases and cancer-induced bone loss, Br. J. Clin. Pharmacol. 85 (6) (2019) 1114–1124, https://doi.org/10.1111/bcp.13852.
[13] L. Bedatsova, M.T. Drake, The skeletal impact of cancer therapies, Br. J. Clin. Pharmacol. 85 (6) (2019) 1161–1168, https://doi.org/10.1111/bcp.13866.
[14] F. Schajowicz, H.A. Sissons, L.H. Sobin, The world health organization's histologic classification of bone tumors. A Commentary on the Second Edition, Cancer 75 (5) (1995) 1208–1214, https://doi.org/10.1002/1097-0142.
[15] J.L. Sottnik, J. Dai, H. Zhang, B. Campbell, E.T. Keller, Tumor-induced pressure in the bone microenvironment causes osteocytes to promote the growth of prostate cancer bone metastases, Cancer Res. 75 (11) (2015) 2151–2158, https://doi.org/10.1158/0008-5472.CAN-14-2493.
[16] L. Lichtenstein, Benign osteoblastoma; A category of osteoid-and bone-forming tumors other than classical osteoid osteoma, which may be mistaken for giant-cell tumor or osteogenic sarcoma, Cancer 9 (5) (1956) 1044–1052, https://doi.org/10.1002/1097-0142(195609/10)9:5<1044::aid-cncr2820090523>3.0.co;2-o.
[17] L. van der Heijden, P.D.S. Dijkstra, J.Y. Blay, H. Gelderblom, Giant cell tumour of bone in the denosumab era, Eur. J. Cancer 77 (2017) 75–83, https://doi.org/10.1016/j.ejca.2017.02.021.
[18] M.S. Isakoff, S.S. Bielack, P. Meltzer, R. Gorlick, Osteosarcoma: current treatment and a collaborative pathway to success, J. Clin. Oncol. 33 (27) (2015) 3029–3035, https://doi.org/10.1200/JCO.2014.59.4895.
[19] M.P. Link, A.M. Goorin, M. Horowitz, W.H. Meyer, J. Belasco, A. Baker, et al., Adjuvant chemotherapy of high-grade osteosarcoma of the extremity. Updated results of the multi-institutional osteosarcoma study, Clin. Orthop. Relat. Res. (270) (1991) 8–14.
[20] S. Smeland, S.S. Bielack, J. Whelan, M. Bernstein, P. Hogendoorn, M.D. Krailo, et al., Survival and prognosis with osteosarcoma: outcomes in more than 2000 patients in the EURAMOS-1 (European and American osteosarcoma study) cohort, Eur. J. Cancer 109 (2019) 36–50, https://doi.org/10.1016/j.ejca.2018.11.027.
[21] A. Cerase, F. Priolo, Skeletal benign bone-forming lesions, Eur. J. Radiol. 27 (Suppl 1) (1998) S91–S97, https://doi.org/10.1016/s0720-048x(98)00049-7.
[22] E.M. Daland, S.M. Wyman, et al., Osteoid osteoma of femur, N. Engl. J. Med. 240 (18) (1949) 728–730, https://doi.org/10.1056/NEJM194905052401806.
[23] M.J. Kransdorf, D.E. Sweet, P.C. Buetow, M.A. Giudici, R.P. Moser Jr., Giant cell tumor in skeletally immature patients, Radiology 184 (1) (1992) 233–237, https://doi.org/10.1148/radiology.184.1.1609086.
[24] U. Bhure, J.E. Roos, K. Strobel, Osteoid osteoma: multimodality imaging with focus on hybrid imaging, Eur. J. Nucl. Med. Mol. Imag. 46 (4) (2019) 1019–1036, https://doi.org/10.1007/s00259-018-4181-2.
[25] P.D. Lester, M. Scott, G.J. Lignelli, F.J. Shea, Osteoid osteoma, JAMA 218 (5) (1971) 741, https://doi.org/10.1001/jama.1971.03190180061029.
[26] R.L. Osborne, The differential radiologic diagnosis of bone tumors. CA, Cancer J. Clin. 24 (4) (1974) 194–211, https://doi.org/10.3322/canjclin.24.4.194.
[27] J.L. Bloem, A.H. Taminiau, F. Eulderink, J. Hermans, E.K. Pauwels, Radiologic staging of primary bone sarcoma: MR imaging, scintigraphy, angiography, and CT correlated with pathologic examination, Radiology 169 (3) (1988) 805–810, https://doi.org/10.1148/radiology.169.3.3055041.
[28] J.L. Bloem, T.H. Falke, A.H. Taminiau, J. Doornbos, A.T. Van Oosterom, R. M. Steiner, et al., Magnetic resonance imaging of primary malignant bone tumors, Radiographics 5 (6) (1985) 853–886, https://doi.org/10.1148/radiographics.5.6.3880008.
[29] L.L. Seeger, R.H. Gold, V.P. Chandnani, Diagnostic imaging of osteosarcoma, Clin. Orthop. Relat. Res. (270) (1991) 254–263.
[30] L. Dercle, R. Chisin, S. Ammari, Q. Gillebert, M. Ouali, C. Jaudet, et al., Nonsurgical giant cell tumour of the tendon sheath or of the diffuse type: are MRI or 18F-FDG PET/CT able to provide an accurate prediction of long-term outcome? Eur. J. Nucl. Med. Mol. Imag. 42 (3) (2015) 397–408, https://doi.org/10.1007/s00259-014-2938-9.
[31] H.J. Lim, C.A. Johnny Ong, J.W. Tan, M.C. Ching Teo, Utility of positron emission tomography/computed tomography (PET/CT) imaging in the evaluation of sarcomas: a systematic review, Crit. Rev. Oncol. Hematol. 143 (2019) 1–13, https://doi.org/10.1016/j.critrevonc.2019.07.002.
[32] E. Bastiaannet, H. Groen, P.L. Jager, D.C. Cobben, W.T. van der Graaf, W. Vaalburg, et al., The value of FDG-PET in the detection, grading and response to therapy of soft tissue and bone sarcomas; a systematic review and meta-analysis, Cancer Treat Rev. 30 (1) (2004) 83–101, https://doi.org/10.1016/j.ctrv.2003.07.004.
[33] M.D. Hurwitz, P. Ghanouni, S.V. Kanaev, D. Iozeffi, D. Gianfelice, F.M. Fennessy, et al., Magnetic resonance-guided focused ultrasound for patients with painful bone metastases: phase III trial results, J. Natl. Cancer Inst. 106 (5) (2014), https://doi.org/10.1093/jnci/dju082.
[34] C. Franzius, H.E. Daldrup-Link, A. Wagner-Bohn, J. Sciuk, W.L. Heindel, H. Jürgens, et al., FDG-PET for detection of recurrences from malignant primary bone tumors: comparison with conventional imaging, Ann. Oncol. 13 (1) (2002) 157–160, https://doi.org/10.1093/annonc/mdf012.
[35] J.R. Ross, Y. Saunders, P.M. Edmonds, S. Patel, K.E. Broadley, S.R. Johnston, Systematic review of role of bisphosphonates on skeletal morbidity in metastatic cancer, Br. Med. J. 327 (7413) (2003) 469, https://doi.org/10.1136/bmj.327.7413.469.
[36] K. Pantel, C. Alix-Panabières, S. Riethdorf, Cancer micrometastases, Nat. Rev. Clin. Oncol. 6 (6) (2009) 339–351, https://doi.org/10.1038/nrclinonc.2009.44.
[37] T. Onishi, N. Hayashi, R.L. Theriault, G.N. Hortobagyi, N.T. Ueno, Future directions of bone-targeted therapy for metastatic breast cancer, Nat. Rev. Clin. Oncol. 7 (11) (2010) 641–651, https://doi.org/10.1038/nrclinonc.2010.134.
[38] J.S. Biermann, W. Chow, D.R. Reed, D. Lucas, D.R. Adkins, M. Agulnik, et al., NCCN guidelines insights: bone cancer, version 2.2017, J. Natl. Compr. Cancer Netw. 15 (2) (2017) 155–167, https://doi.org/10.6004/jnccn.2017.0017.
[39] A. Matsumine, K. Kusuzaki, T. Matsubara, A. Okamura, N. Okuyama, S. Miyazaki, et al., Calcium phosphate cement in musculoskeletal tumor surgery, J. Surg. Oncol. 93 (3) (2006) 212–220, https://doi.org/10.1002/jso.20355.
[40] M. Yasuda, K. Masada, E. Takeuchi, Treatment of enchondroma of the hand with injectable calcium phosphate bone cement, J. Hand Surg. Am. 31 (1) (2006) 98–102, https://doi.org/10.1016/j.jhsa.2005.08.017.
[41] W. Wang, K.W.K. Yeung, Bone grafts and biomaterials substitutes for bone defect repair: a review, Bioact. Mater. 2 (4) (2017) 224–247, https://doi.org/10.1016/j.bioactmat.2017.05.007.
[42] S.M. Kenny, M. Buggy, Bone cements and fillers: a review, J. Mater. Sci. Mater. Med. 14 (11) (2003) 923–938, https://doi.org/10.1023/a:1026394530192.
[43] A.K. Ray, J.S. Romine, A.M. Pankovich, Stabilization of pathologic fractures with acrylic cement, Clin. Orthop. Relat. Res. 101 (1974) 182–185.
[44] H.H. Xu, P. Wang, L. Wang, C. Bao, Q. Chen, M.D. Weir, et al., Calcium phosphate cements for bone engineering and their biological properties, Bone Res 5 (2017), 17056, https://doi.org/10.1038/boneres.2017.56.
[45] T. Fujibuchi, S. Matsumoto, T. Shimoji, K. Ae, T. Tanizawa, T. Gokita, et al., New endoprosthesis suspension method with polypropylene monofilament knitted mesh after resection of bone tumors in proximal humerus, J. Shoulder Elbow Surg. 24 (6) (2015) 882–888, https://doi.org/10.1016/j.jse.2014.10.011.
[46] K.M. Winters-Stone, A.L. Schwartz, S.C. Hayes, C.J. Fabian, K.L. Campbell, A prospective model of care for breast cancer rehabilitation: bone health and arthralgias, Cancer 118 (8 Suppl) (2012) 2288–2299, https://doi.org/10.1002/cncr.27465.
[47] W.H. Isacoff, C.M. Townsend, F.R. Eiber, T. Forster, D.L. Morton, J.B. Block, High dose methotrexate therapy of solid tumors: observations relating to clinical

toxicity, Pediatr. Blood Cancer 2 (3) (1976) 319–325, https://doi.org/10.1002/mpo.2950020313.
[48] G. Rosen, B. Caparros, A.G. Huvos, C. Kosloff, A. Nirenberg, A. Cacavio, et al., Preoperative chemotherapy for osteogenic sarcoma: selection of postoperative adjuvant chemotherapy based on the response of the primary tumor to preoperative chemotherapy, Cancer 49 (6) (1982) 1221–1230, https://doi.org/10.1002/1097-0142.
[49] F. Saad, D. Cella, E. Basch, B.A. Hadaschik, P.N. Mainwaring, S. Oudard, et al., Effect of apalutamide on health-related quality of life in patients with non-metastatic castration-resistant prostate cancer: an analysis of the SPARTAN randomised, placebo-controlled, phase 3 trial, Lancet Oncol. 19 (10) (2018) 1404–1416, https://doi.org/10.1016/S1470-2045(18)30456-X.
[50] K. Fizazi, H.I. Scher, K. Miller, E. Basch, C.N. Sternberg, D. Cella, et al., Effect of enzalutamide on time to first skeletal-related event, pain, and quality of life in men with castration-resistant prostate cancer: results from the randomised, phase 3 AFFIRM trial, Lancet Oncol. 15 (10) (2014) 1147–1156, https://doi.org/10.1016/S1470-2045(14)70303-1.
[51] R. Mhaskar, A. Kumar, B. Miladinovic, B. Djulbegovic, Bisphosphonates in multiple myeloma: an updated network meta-analysis, Cochrane Database Syst. Rev. 12 (12) (2017), Cd003188, https://doi.org/10.1002/14651858.CD003188.pub4.
[52] M. Yilmaz, M.S. Sorensen, C. Saebye, T. Baad-Hansen, M.M. Petersen, Long-term results of the global modular replacement system tumor prosthesis for reconstruction after limb-sparing bone resections in orthopedic oncologic conditions: results from a national cohort, J. Surg. Oncol. 120 (2) (2019) 183–192, https://doi.org/10.1002/jso.25490.
[53] K. Zheng, X.C. Yu, Y.C. Hu, Z.W. Shao, M. Xu, B.C. Wang, et al., Outcome of segmental prosthesis reconstruction for diaphyseal bone tumors: a multi-center retrospective study, BMC Cancer 19 (1) (2019) 638, https://doi.org/10.1186/s12885-019-5865-0.
[54] D. Donati, M. Colangeli, S. Colangeli, C. Di Bella, M. Mercuri, Allograft-prosthetic composite in the proximal tibia after bone tumor resection, Clin. Orthop. Relat. Res. 466 (2) (2008) 459–465, https://doi.org/10.1007/s11999-007-0055-9.
[55] H.J. Mankin, M.C. Gebhardt, L.C. Jennings, D.S. Springfield, W.W. Tomford, Long-term results of allograft replacement in the management of bone tumors, Clin. Orthop. Relat. Res. 324 (1996), https://doi.org/10.1097/00003086-199603000-00011.
[56] D.N. Bracey, N.E. Cignetti, A.H. Jinnah, A.V. Stone, B.M. Gyr, P.W. Whitlock, et al., Bone xenotransplantation: a review of the history, orthopedic clinical literature, and a single-center case series, Xenotransplantation 27 (5) (2020), e12600, https://doi.org/10.1111/xen.12600.
[57] S. Ghanaati, M. Barbeck, J. Lorenz, S. Stuebinger, O. Seitz, C. Landes, et al., Synthetic bone substitute material comparable with xenogeneic material for bone tissue regeneration in oral cancer patients: first and preliminary histological, histomorphometrical and clinical results, Ann. Maxillofac. Surg. 3 (2) (2013) 126–138, https://doi.org/10.4103/2231-0746.119221.
[58] G. Fernandez de Grado, L. Keller, Y. Idoux-Gillet, Q. Wagner, A.M. Musset, N. Benkirane-Jessel, et al., Bone substitutes: a review of their characteristics, clinical use, and perspectives for large bone defects management, J. Tissue Eng. 9 (2018), 2041731418776819, https://doi.org/10.1177/2041731418776819.
[59] M.P. Ginebra, C. Canal, M. Espanol, D. Pastorino, E.B. Montufar, Calcium phosphate cements as drug delivery materials, Adv. Drug Deliv. Rev. 64 (12) (2012) 1090–1110, https://doi.org/10.1016/j.addr.2012.01.008.
[60] K. Kurashina, A. Ogiso, A. Kotani, H. Takeuchi, M. Hirano, Histological and microradiographic evaluation of hydrated and hardened alpha-tricalcium phosphate/calcium phosphate dibasic mixtures, Biomaterials 15 (6) (1994) 429–432, https://doi.org/10.1016/0142-9612(94)90221-6.
[61] D. Apelt, F. Theiss, A.O. El-Warrak, K. Zlinszky, R. Bettschart-Wolfisberger, M. Bohner, et al., In vivo behavior of three different injectable hydraulic calcium phosphate cements, Biomaterials 25 (7-8) (2004) 1439–1451, https://doi.org/10.1016/j.biomaterials.2003.08.073.
[62] A. Uchida, N. Araki, Y. Shinto, H. Yoshikawa, E. Kurisaki, K. Ono, The use of calcium hydroxyapatite ceramic in bone tumour surgery, J. Bone Joint Surg. Br. 72 (2) (1990) 298–302, https://doi.org/10.1302/0301-620X.72B2.2155908.
[63] H. Yoshikawa, N. Tamai, T. Murase, A. Myoui, Interconnected porous hydroxyapatite ceramics for bone tissue engineering, J. R. Soc. Interface 6 (Suppl 3) (2009) S341–S348, https://doi.org/10.1098/rsif.2008.0425.focus.
[64] Y. Lu, G. Chen, Z. Long, M. Li, C. Ji, F. Wang, et al., Novel 3D-printed prosthetic composite for reconstruction of massive bone defects in lower extremities after malignant tumor resection, J. Bone. Oncol. 16 (2019), 100220, https://doi.org/10.1016/j.jbo.2019.100220.
[65] Y.H. Liang, H.B. He, C. Zhang, Y.P. Liu, J. Wan, Epiphyseal distraction and hybrid reconstruction using polymethyl methacrylate construct combined with free non-vascularized fibular graft in pediatric patients with osteosarcoma around knee: a case report, World J. Clin. Cases. 7 (21) (2019) 3632–3638, https://doi.org/10.12998/wjcc.v7.i21.3632.
[66] J. Benevenia, S.M. Rivero, J. Moore, J.A. Ippolito, D.A. Siegerman, K.S. Beebe, et al., Supplemental bone grafting in giant cell tumor of the extremity reduces nononcologic complications, Clin. Orthop. Relat. Res. 475 (3) (2017) 776–783, https://doi.org/10.1007/s11999-016-4755-x.
[67] H. Tsuchiya, K. Tomita, Prognosis of osteosarcoma treated by limb-salvage surgery: the ten-year intergroup study in Japan, Jpn. J. Clin. Oncol. 22 (5) (1992) 347–353.
[68] K.H. Shin, B.T. Rougraff, M.A. Simon, Oncologic outcomes of primary bone sarcomas of the pelvis, Clin. Orthop. Relat. Res. (304) (1994) 207–217.
[69] J.-J. Body, M. Pot, A. Borkowski, J.-P. Sculier, J. Klastersky, Dose/response study of aminohydroxypropylidene bisphosphonate in tumor-associated hypercalcemia, Am. J. Med. 82 (5) (1987) 957–963, https://doi.org/10.1016/0002-9343(87)90158-6.
[70] J.H. Healey, F. Shannon, P. Boland, G.R. DiResta, PMMA to stabilize bone and deliver antineoplastic and antiresorptive agents, Clin. Orthop. Relat. Res. (415 Suppl) (2003) S263–S275, https://doi.org/10.1097/01.blo.0000093053.96273.ee.
[71] C. Marques, J.M. Ferreira, E. Andronescu, D. Ficai, M. Sonmez, A. Ficai, Multifunctional materials for bone cancer treatment, Int. J. Nanomed. 9 (2014) 2713–2725, https://doi.org/10.2147/IJN.S55943.
[72] A. Di Martino, M. Sittinger, M.V. Risbud, Chitosan: a versatile biopolymer for orthopaedic tissue-engineering, Biomaterials 26 (30) (2005) 5983–5990, https://doi.org/10.1016/j.biomaterials.2005.03.016.
[73] R.A. Muzzarelli, M. Mattioli-Belmonte, C. Tietz, R. Biagini, G. Ferioli, M. A. Brunelli, et al., Stimulatory effect on bone formation exerted by a modified chitosan, Biomaterials 15 (13) (1994) 1075–1081, https://doi.org/10.1016/0142-9612(94)90093-0.
[74] X. Yang, X. Chen, H. Wang, Acceleration of osteogenic differentiation of preosteoblastic cells by chitosan containing nanofibrous scaffolds, Biomacromolecules 10 (10) (2009) 2772–2778, https://doi.org/10.1021/bm900623j.
[75] L. Liu, Y. He, X. Shi, H. Gao, Y. Wang, Z. Lin, Phosphocreatine-modified chitosan porous scaffolds promote mineralization and osteogenesis in vitro and in vivo, Appl. Mater. Today 12 (2018) 21–33, https://doi.org/10.1016/j.apmt.2018.03.010.
[76] M.L. Tan, P. Shao, A.M. Friedhuber, M. van Moorst, M. Elahy, S. Indumathy, et al., The potential role of free chitosan in bone trauma and bone cancer management, Biomaterials 35 (27) (2014) 7828–7838, https://doi.org/10.1016/j.biomaterials.2014.05.087.
[77] Y.C. Lin, P.J. Lou, T.H. Young, Chitosan as an adjuvant-like substrate for dendritic cell culture to enhance antitumor effects, Biomaterials 35 (31) (2014) 8867–8875, https://doi.org/10.1016/j.biomaterials.2014.07.014.
[78] M. Vallet-Regí, E. Ruiz-Hernández, Bioceramics: from bone regeneration to cancer nanomedicine, Adv. Mater. 23 (44) (2011) 5177–5218, https://doi.org/10.1002/adma.201101586.
[79] K. Zhang, Y. Zhou, Application of hydroxyapatite nanoparticles in tumor-associated bone segmental defect, Sci. Adv. 5 (8) (2019), eaax6946, https://doi.org/10.1126/sciadv.aax6946.
[80] S.R. Prasad, T.S.S. Kumar, A. Jayakrishnan, Ceramic core with polymer corona hybrid nanocarrier for the treatment of osteosarcoma with Co-delivery of protein and anti-cancer drug, Nanotechnology 29 (1) (2017), 015101, https://doi.org/10.1088/1361-6528/aa9a21.
[81] I. Bischoff, R. Tsaryk, F. Chai, R. Fürst, C.J. Kirkpatrick, R.E. Unger, In vitro evaluation of a biomaterial-based anticancer drug delivery system as an alternative to conventional post-surgery bone cancer treatment, Mater. Sci. Eng. C 93 (2018) 115–124, https://doi.org/10.1016/j.msec.2018.07.057.
[82] A. Luetke, P.A. Meyers, I. Lewis, H. Juergens, Osteosarcoma treatment - where do we stand? A state of the art review, Cancer Treat Rev. 40 (4) (2014) 523–532, https://doi.org/10.1016/j.ctrv.2013.11.006.
[83] M. Sun, M. Wang, M. Chen, F. Dagnaes-Hansen, D.Q.S. Le, A. Baatrup, et al., A tissue-engineered therapeutic device inhibits tumor growth in vitro and in vivo, Acta Biomater. 18 (2015) 21–29, https://doi.org/10.1016/j.actbio.2015.02.004.
[84] Y. Liu, A. Nadeem, S. Sebastian, M.A. Olsson, S.N. Wai, E. Styring, et al., Bone mineral: a trojan horse for bone cancers. Efficient mitochondria targeted delivery and tumor eradication with nano hydroxyapatite containing doxorubicin, Mater. Today Bio. 14 (2022), 100227, https://doi.org/10.1016/j.mtbio.2022.100227.
[85] C. Wang, X.Y. Ye, Y.T. Zhao, L. Bai, Z. He, Q. Tong, et al., Cryogenic 3D printing of porous scaffolds for in situ delivery of 2D black phosphorus nanosheets, doxorubicin hydrochloride and osteogenic peptide for treating tumor resection-induced bone defects, Biofabrication 12 (3) (2020), https://doi.org/10.1088/1758-5090/ab6d35.
[86] X.Z. Liu, H.B. Zhang, R.Y. Cheng, Y.Z. Gu, Y. Yin, Z.Y. Sun, et al., An immunological electrospun scaffold for tumor cell killing and healthy tissue regeneration, Mater. Horiz. 5 (6) (2018) 1082–1091, https://doi.org/10.1039/c8mh00704g.
[87] M.R. Junttila, F.J. de Sauvage, Influence of tumour micro-environment heterogeneity on therapeutic response, Nature 501 (7467) (2013) 346–354, https://doi.org/10.1038/nature12626.
[88] M. López-Lázaro, Dual role of hydrogen peroxide in cancer: possible relevance to cancer chemoprevention and therapy, Cancer Lett. 252 (1) (2007) 1–8, https://doi.org/10.1016/j.canlet.2006.10.029.
[89] B. Kumar, S. Koul, L. Khandrika, R.B. Meacham, H.K. Koul, Oxidative stress is inherent in prostate cancer cells and is required for aggressive phenotype, Cancer Res. 68 (6) (2008) 1777–1785, https://doi.org/10.1158/0008-5472.CAN-07-5259.
[90] L.Y. Wang, Q.H. Yang, M.F. Huo, D. Lu, Y.S. Gao, Y. Chen, et al., Engineering single-atomic iron-catalyst-integrated 3D-printed bioscaffolds for osteosarcoma destruction with antibacterial and bone defect regeneration bioactivity, Adv. Mater. 33 (31) (2021), https://doi.org/10.1002/adma.202100150.
[91] Y. Zhang, Q. Zhang, F. Wang, M. Li, X. Shi, J. Li, Activatable semiconducting polymer nanoinducers amplify oxidative damage via sono-ferroptosis for synergistic therapy of bone metastasis, Nano Lett. 23 (16) (2023) 7699–7708, https://doi.org/10.1021/acs.nanolett.3c02414.
[92] S. Dong, Y. Chen, L. Yu, K. Lin, X. Wang, Magnetic hyperthermia–synergistic H_2O_2 self-sufficient catalytic suppression of osteosarcoma with enhanced bone-

regeneration bioactivity by 3D-printing composite scaffolds, Adv. Funct. Mater. 30 (4) (2020), 1907071, https://doi.org/10.1002/adfm.201907071.
[93] H. Ma, T. Li, Z. Huan, M. Zhang, Z. Yang, J. Wang, et al., 3D printing of high-strength bioscaffolds for the synergistic treatment of bone cancer, NPG Asia Mater. 10 (4) (2018) 31–44, https://doi.org/10.1038/s41427-018-0015-8.
[94] L. Pang, R. Zhao, J. Chen, J. Ding, X. Chen, W. Chai, et al., Osteogenic and anti-tumor Cu and Mn-doped borosilicate nanoparticles for syncretic bone repair and chemodynamic therapy in bone tumor treatment, Bioact. Mater. 12 (2022) 1–15, https://doi.org/10.1016/j.bioactmat.2021.10.030.
[95] J. Overgaard, History and heritage: an introduction, Hyperthermic Oncol. 2 (1985) 8–9.
[96] O.S. Nielsen, M. Horsman, J. Overgaard, A future for hyperthermia in cancer treatment? Eur. J. Cancer 37 (13) (2001) 1587–1589, https://doi.org/10.1016/s0959-8049(01)00193-9.
[97] J. Overgaard, Effect of hyperthermia on malignant cells in vivo. A review and a hypothesis, Cancer 39 (6) (1977) 2637–2646, https://doi.org/10.1002/1097-0142.
[98] B. Tan, Y. Wu, Y. Wu, K. Shi, R. Han, Y. Li, et al., Curcumin-Microsphere/IR820 hybrid bifunctional hydrogels for in situ osteosarcoma chemo-co-thermal therapy and bone reconstruction, ACS Appl. Mater. Interfaces 13 (27) (2021) 31542–31553, https://doi.org/10.1021/acsami.1c08775.
[99] Y. Liu, R. Lin, L. Ma, H. Zhuang, C. Feng, J. Chang, et al., Mesoporous bioactive glass for synergistic therapy of tumor and regeneration of bone tissue, Appl. Mater. Today 19 (2020), 100578, https://doi.org/10.1016/j.apmt.2020.100578.
[100] C. Li, W. Zhang, R. Wang, X.-F. Du, D. Jiang, B. Liu, et al., Nanocomposite multifunctional hydrogel for suppressing osteosarcoma recurrence and enhancing bone regeneration, J. Chem. Eng. 435 (2022), 134896, https://doi.org/10.1016/j.cej.2022.134896.
[101] H. Ma, J. Luo, Z. Sun, L. Xia, M. Shi, M. Liu, et al., 3D printing of biomaterials with mussel-inspired nanostructures for tumor therapy and tissue regeneration, Biomaterials 111 (2016) 138–148, https://doi.org/10.1016/j.biomaterials.2016.10.005.
[102] S. Luo, J. Wu, Z. Jia, P. Tang, J. Sheng, C. Xie, et al., An injectable, bifunctional hydrogel with photothermal effects for tumor therapy and bone regeneration, Macromol. Biosci. 19 (9) (2019), e1900047, https://doi.org/10.1002/mabi.201900047.
[103] H. Lin, S. Shi, X. Lan, X. Quan, Q. Xu, G. Yao, et al., Scaffold 3D-printed from metallic nanoparticles-containing ink simultaneously eradicates tumor and repairs tumor-associated bone defects, Small Methods 5 (9) (2021), e2100536, https://doi.org/10.1002/smtd.202100536.
[104] S. Dong, Y.N. Zhang, J. Wan, R. Cui, X. Yu, G. Zhao, et al., A novel multifunctional carbon aerogel-coated platform for osteosarcoma therapy and enhanced bone regeneration, J. Mater. Chem. B 8 (3) (2020) 368–379, https://doi.org/10.1039/c9tb02383f.
[105] Y. Lu, L. Li, M. Li, Z. Lin, L. Wang, Y. Zhang, et al., Zero-dimensional carbon dots enhance bone regeneration, osteosarcoma ablation, and clinical bacterial eradication, Bioconjugate Chem. 29 (9) (2018) 2982–2993, https://doi.org/10.1021/acs.bioconjchem.8b00400.
[106] S. Fu, H. Hu, J. Chen, Y. Zhu, S. Zhao, Silicone resin derived larnite/C scaffolds via 3D printing for potential tumor therapy and bone regeneration, J. Chem. Eng. 382 (2020), 122928, https://doi.org/10.1016/j.cej.2019.122928.
[107] C. Zhao, A. Shen, L. Zhang, K. Lin, X. Wang, Borocarbonitrides nanosheets engineered 3D-printed scaffolds for integrated strategy of osteosarcoma therapy and bone regeneration, J. Chem. Eng. 401 (2020), 125989, https://doi.org/10.1016/j.cej.2020.125989.
[108] H.S. Ma, C.A. Jiang, D. Zhai, Y.X. Luo, Y. Chen, F. Lv, et al., A bifunctional biomaterial with photothermal effect for tumor therapy and bone regeneration, Adv. Funct. Mater. 26 (8) (2016) 1197–1208, https://doi.org/10.1002/adfm.201504142.
[109] Y.W. Ge, X.L. Liu, D.G. Yu, Z.A. Zhu, Q.F. Ke, Y.Q. Mao, et al., Graphene-modified $CePO_4$ nanorods effectively treat breast cancer-induced bone metastases and regulate macrophage polarization to improve osteo-inductive ability, J. Nanobiotechnol. 19 (1) (2021) 11, https://doi.org/10.1186/s12951-020-00753-9.
[110] L. Ma, X. Feng, H. Liang, K. Wang, Y. Song, L. Tan, et al., A novel photothermally controlled multifunctional scaffold for clinical treatment of osteosarcoma and tissue regeneration, Mater. Today 36 (2020) 48–62, https://doi.org/10.1016/j.mattod.2019.12.005.
[111] S.S. Pan, J.H. Yin, L.D. Yu, C.Q. Zhang, Y.F. Zhu, Y.S. Gao, et al., 2D MXene-integrated 3D-printing scaffolds for augmented osteosarcoma phototherapy and accelerated tissue reconstruction, Adv. Sci. 7 (2) (2020), https://doi.org/10.1002/advs.201901511.
[112] J. Yin, S. Pan, X. Guo, Y. Gao, D. Zhu, Q. Yang, et al., Nb_2C MXene-functionalized scaffolds enables osteosarcoma phototherapy and angiogenesis/osteogenesis of bone defects, Nano-Micro Lett. 13 (1) (2021) 30, https://doi.org/10.1007/s40820-020-00547-6.
[113] Q.H. Yang, H.H. Yin, T.M. Xu, D.Y. Zhu, J.H. Yin, Y.X. Chen, et al., Engineering 2D mesoporous Silica@MXene-integrated 3D-printing scaffolds for combinatory osteosarcoma therapy and NO-augmented bone regeneration, Small 16 (14) (2020), https://doi.org/10.1002/smll.201906814.
[114] C. He, L.D. Yu, H.L. Yao, Y. Chen, Y.Q. Hao, Combinatorial photothermal 3D-printing scaffold and checkpoint blockade inhibits growth/metastasis of breast cancer to bone and accelerates osteogenesis, Adv. Funct. Mater. 31 (10) (2021), https://doi.org/10.1002/adfm.202006214.
[115] J. Long, W. Zhang, Y. Chen, B. Teng, B. Liu, H. Li, et al., Multifunctional magnesium incorporated scaffolds by 3D-printing for comprehensive postsurgical management of osteosarcoma, Biomaterials 275 (2021), 120950, https://doi.org/10.1016/j.biomaterials.2021.120950.
[116] A.R. Rastinehad, H. Anastos, E. Wajswol, J.S. Winoker, J.P. Sfakianos, S. K. Doppalapudi, et al., Gold nanoshell-localized photothermal ablation of prostate tumors in a clinical pilot device study, Proc. Natl. Acad. Sci. U.S.A. 116 (37) (2019) 18590–18596, https://doi.org/10.1073/pnas.1906929116.
[117] J. Liao, K. Shi, Y. Jia, Y. Wu, Z. Qian, Gold nanorods and nanohydroxyapatite hybrid hydrogel for preventing bone tumor recurrence via postoperative photothermal therapy and bone regeneration promotion, Bioact. Mater. 6 (8) (2021) 2221–2230, https://doi.org/10.1016/j.bioactmat.2021.01.006.
[118] Z. Yang, F.J. Zhao, W. Zhang, Z.Y. Yang, M. Luo, L. Liu, et al., Degradable photothermal bioactive glass composite hydrogel for the sequential treatment of tumor-related bone defects: from anti-tumor to repairing bone defects, J. Chem. Eng. 419 (2021), https://doi.org/10.1016/j.cej.2021.129520.
[119] Y. Liu, T. Li, H. Ma, D. Zhai, C. Deng, J. Wang, et al., 3D-printed scaffolds with bioactive elements-induced photothermal effect for bone tumor therapy, Acta Biomater. 73 (2018) 531–546, https://doi.org/10.1016/j.actbio.2018.04.014.
[120] W. Dang, T. Li, B. Li, H. Ma, D. Zhai, X. Wang, et al., A bifunctional scaffold with $CuFeSe_2$ nanocrystals for tumor therapy and bone reconstruction, Biomaterials 160 (2018) 92–106, https://doi.org/10.1016/j.biomaterials.2017.11.020.
[121] B.W. Yang, J.H. Yin, Y. Chen, S.S. Pan, H.L. Yao, Y.S. Gao, et al., 2D-Black-Phosphorus-Reinforced 3D-printed scaffolds:A stepwise countermeasure for osteosarcoma, Adv. Mater. 30 (10) (2018), https://doi.org/10.1002/adma.201705611.
[122] X.C. Wang, T. Li, H.S. Ma, D. Zhai, C. Jiang, J. Chang, et al., A 3D-printed scaffold with MoS_2 nanosheets for tumor therapy and tissue regeneration, NPG Asia Mater. 9 (2017), https://doi.org/10.1038/am.2017.47.
[123] C. He, C. Dong, L. Yu, Y. Chen, Y. Hao, Ultrathin 2D inorganic ancient pigment decorated 3D-printing scaffold enables photonic hyperthermia of osteosarcoma in NIR-II biowindow and concurrently augments bone regeneration, Adv. Sci. 8 (19) (2021), e2101739, https://doi.org/10.1002/advs.202101739.
[124] W.T. Dang, B. Ma, B. Li, Z.G. Huan, N. Ma, H.B. Zhu, et al., 3D printing of metal-organic framework nanosheets-structured scaffolds with tumor therapy and bone construction, Biofabrication 12 (2) (2020), https://doi.org/10.1088/1758-5090/ab5ae3.
[125] Y. Qu, H. Zhuang, M. Zhang, Y. Wang, D. Zhai, B. Ma, et al., Bone cements for therapy and regeneration for minimally invasive treatment of neoplastic bone defects, J. Mater. Chem. B 9 (21) (2021) 4355–4364, https://doi.org/10.1039/d1tb00703c.
[126] C. Yang, H. Ma, Z. Wang, M.R. Younis, C. Liu, C. Wu, et al., 3D printed wesselsite nanosheets functionalized scaffold facilitates NIR-II photothermal therapy and vascularized bone regeneration, Adv. Sci. 8 (20) (2021), e2100894, https://doi.org/10.1002/advs.202100894.
[127] H. Zhuang, C. Qin, M. Zhang, J. Ma, D. Zhai, B. Ma, et al., 3D-printed bioceramic scaffolds with Fe_3S_4microflowers for magnetothermal and chemodynamic therapy of bone tumor and regeneration of bone defects, Biofabrication 13 (4) (2021), https://doi.org/10.1088/1758-5090/ac19c7.
[128] A. Matsumine, K. Takegami, K. Asanuma, T. Matsubara, T. Nakamura, A. Uchida, et al., A novel hyperthermia treatment for bone metastases using magnetic materials, Int. J. Clin. Oncol. 16 (2) (2011) 101–108, https://doi.org/10.1007/s10147-011-0217-3.
[129] J.J. Mack, B.N. Cox, O. Sudre, A.A. Corrin, S.L. dos Santos e Lucato, C. Ma, et al., Achieving nutrient pumping and strain stimulus by magnetic actuation of tubular scaffolds, Smart Mater. Struct. 18 (10) (2009), 104025, https://doi.org/10.1088/0964-1726/18/10/104025.
[130] S.J. Dong, Y. Chen, L.D. Yu, K.L. Lin, X.D. Wang, Magnetic hyperthermia-synergistic H_2O_2 self-sufficient catalytic suppression of osteosarcoma with enhanced bone-regeneration bioactivity by 3D-printing composite scaffolds, Adv. Funct. Mater. 30 (4) (2020), https://doi.org/10.1002/adfm.201907071.
[131] F. Yang, J. Lu, Q. Ke, X. Peng, Y. Guo, X. Xie, Magnetic mesoporous calcium sillicate/chitosan porous scaffolds for enhanced bone regeneration and photothermal-chemotherapy of osteosarcoma, Sci. Rep. 8 (1) (2018) 7345, https://doi.org/10.1038/s41598-018-25595-2.
[132] J.W. Lu, F. Yang, Q.F. Ke, X.T. Xie, Y.P. Guo, Magnetic nanoparticles modified-porous scaffolds for bone regeneration and photothermal therapy against tumors, Nanomed. Nanotechnol. Biol. Med. 14 (3) (2018) 811–822, https://doi.org/10.1016/j.nano.2017.12.025.
[133] F.F. Yan, Z.B. Liu, T. Zhang, Q. Zhang, Y. Chen, Y.L. Xie, et al., Biphasic injectable bone cement with Fe_3O_4/GO nanocomposites for the minimally invasive treatment of tumor-induced bone destruction, ACS Biomater. Sci. Eng. 5 (11) (2019) 5833–5843, https://doi.org/10.1021/acsbiomaterials.9b00472.